

# THE MSC50 WIND AND WAVE REANALYSIS

V.R Swail<sup>1</sup>, V.J. Cardone<sup>2</sup>, M. Ferguson<sup>2</sup>, D.J. Gummer<sup>2</sup>,  
E.L. Harris<sup>2</sup>, E.A. Orelup<sup>2</sup> and A.T. Cox<sup>2</sup>

<sup>1</sup>Environment Canada  
Toronto, Ontario

<sup>2</sup>Oceanweather, Inc.  
Cos Cob, CT

## 1. INTRODUCTION

About four decades ago the offshore industry began in earnest to seek and develop energy resources in particularly harsh marine environments, such as the North Sea, which is visited frequently by severe extratropical cyclones, and the Gulf of Mexico, in which intense tropical cyclones may occur in any given year. With the discovery of the giant Hibernia oil field offshore Newfoundland in the mid-1970s and other finds offshore Nova Scotia soon thereafter, the need for high quality design Metocean data as required for the reliable, safe and cost effective design of offshore infrastructure extended to these areas as well. The so-called hindcast approach emerged during these relatively early years as the only reliable method available to specify Metocean design data in a rational and objective way. The hindcast approach consists of the application of numerical wind and wave models together with historical meteorological data to simulate the evolution of surface winds and ocean wave response in the basin or region of interest. Application of the statistical process of extremal analysis to the hindcast data at specific sites yields the design criteria (e.g. 100-year return period significant wave height) required by structural engineers.

The study reported here addresses the North Atlantic (NA) basin so it is interesting to review the evolution of application of the hindcast approach in this basin leading up to the MSC50. The first hindcast study (actually a study and its update) was carried out by Oceanweather Inc. for Mobil Research and Development Corporation (1982-86) to provide the first design estimates for Hibernia (see e.g. Cardone et al., 1989). The labor-intensity of the wind field analysis process and computer speeds limited the hindcast to a total of 29 severe storms occurring between January 1951 and December 1984. Storms were identified mainly by examining historical surface weather maps but that process was somewhat subjective and it was found after the hindcast that about 10% of the storms selected were too weak to belong to the intended population. Winds were first calculated from hand-

drawn pressure maps based on synoptic measurements that were available in real-time. These were then modified through kinematic analysis and the inclusion of pressure and wind data not reported in real-time. Waves were hindcast using the ODGP (Ocean Data Gathering Project) model adapted on grids with a typical spacing of 2 degree latitude by 2 degree longitude covering only the western two-thirds of the NA. The study produced a nominal mean 100-year HS of 14.4 m with the upper 90% confidence limit at 15.9 m, which was the value selected by Mobil to account for the uncertainty in the estimate.

The second study, supported by PERD (Program of Energy Research and Development), was intended to develop a hindcast data base and extreme wave estimates for the entire Canadian east coast offshore exploration areas including the Grand Banks, the Scotian Shelf, and Georges Bank (see Swail et al., 1989). The time period covered in the storm selection process was 1957 – 1988. A total of 68 storms covering the three areas were included in the study. Interestingly, it was found that the PERD storm population for the period overlapping the Hibernia study included several storms that exceeded in intensity the threshold implied by the Hibernia population, thereby further demonstrating the difficulty of identifying and ranking historical storms solely from examination of conventional weather maps and marine observations. The winds were modeled using a blend of surface pressure analysis and kinematic analysis wind fields. Waves were hindcast using a deepwater ODGP wave model. A nested model grid was used with the coarse grid spacing of 1.25° latitude by 2.5° longitude extending from 25° N to 67.5° N and 20° W to 80° W, and a fine grid of half the spacing of the coarse and covering the area between 38.75° N to 53.75° N and 42.5° W to the coast.

A third study was performed in 1995 and 1996 as an update to the PERD study wherein the time period of the hindcast was extended and a third-generation (3G) wave model was applied with the inclusion of shallow

water physics for the first time. 82 storms were hindcast covering the time period from 1957 to 1995. A nested grid was used having a coarse grid spacing of  $1.084^\circ$  longitude on the assumed equator (at  $51^\circ\text{W}$ ) and a nested fine grid with spacing of about  $0.361^\circ$  of longitude. This study is described by Swail et al, 1995.

Beginning in the 1990s, computer speed had increased sufficiently to allow some hindcast studies to include the simulation of continuous multiyear periods, typically 10-years or less, from which operational wind and wave criteria could be developed, such as scatter diagrams and persistence/duration statistics. However, the underlying source wind fields were typically of low spatial resolution, highly smoothed and in some cases biased. The limitations of continuous hindcasts were addressed in the landmark AES40 study, which modeled initially the entire 40 year time period from 1958 to 1997, and was eventually updated to include July, 1, 1954 to June 30, 2004 (600 months). The study utilized the results of the NCAR/NCEP (National Center for Atmospheric Research/U.S. National Centers for Environmental Prediction) global re-analysis for 1958-97 wind fields as input to a third generation deep water wave model. The winds were modified by adding measured winds from high quality buoys, platforms, and C-MAN stations. Tropical cyclone wind fields were also generated and added to the background winds. Lastly, the wind fields were refined using Oceanweather's Interactive Objective Kinematic Analysis System (IOKA) (Cox *et al.*, 1995). A 3G wave model was adapted to the entire NA on a grid of spacing  $0.625^\circ$  latitude by  $0.833^\circ$  longitude. The veracity of the hindcast was evaluated against all high quality in-situ wave measurements available during the hindcast period and all satellite altimeter wind speed and wave height measurements. Concurrently with the AES40 hindcast, the first global wave hindcast based on the NCAR/NCEP, called GROW (Cox and Swail, 2001) became available and was soon joined by several alternative efforts. Caires et al. (2004) intercompared these modern continuous hindcast databases and carried out an independent verification of the hindcast wind speeds and wave heights against in-situ and satellite altimeter data. It was concluded that in the NA, AES40 best represents the measurements and was recommended as the reference database for the NA.

The purpose of MSC50 project was to improve AES40 by modeling the Canadian East Coast at significantly higher resolution while including shallow water physics in the same 3G model applied in AES40, increase the spatial resolution of the basin-grid as well, and increase the temporal resolution of the archive, increase accuracy in order to reduce the uncertainty in

any climate or design data statistics produced from the hindcast database.

## 2. METHODOLOGY

The MSC50 project followed the same basic methodology as was applied in the AES40 hindcast with notable improvements and upgrades. One of the challenges in the MSC50 was to identify areas of improvement that could be made over the original hindcast. The AES40 employed over 10,000 meteorologist hours of analysis and has been extensively validated by both internal (Swail et al. 2000) and external (Woolf et al. 2002, Caires et al. 2004) groups and found to possess excellent skill.

### 2.1 Wind Fields

One of the key components of the AES40 hindcast was the reanalysis of surface winds. This reanalysis involved a skilled marine meteorologist applying a graphical user interface known as the Wind WorkStation (WWS, Cox et al. 1995) Surface fields were reviewed on a 6-hourly basis and special attention was paid to the evolution of significant storms.

The MSC50 applied the latest generation WWS which incorporated new dynamic repositioning of marine data and for the first time allowed direct kinematic analysis of isotachs and/or streamlines within the toolset. One deficiency identified in the AES40 was in the use of 6-hourly analysis during rapidly developing winter storms off the U.S. New England coastline. These storms would intensify rapidly in the Gulf of Maine and then track over Canadian waters. In the MSC50, these systems were addressed with a 3-hourly analysis timestep to better capture these systems. Original 6-hourly NCEP/NCAR 10-meter wind fields were time interpolated using a moving centers interpolation algorithm which maintains the spatial characteristics of a storm without "smearing" the solution. The moving centers were derived from the NCEP/NCAR sea level pressures with manual shifting of the centers to ensure a smooth track. These moving centers were also applied in the dynamic repositioning of off-hour data. This repositioning allows better use of the US and Canadian buoy arrays during storm periods and was also very useful for asynoptic fields such as scatterometer winds. Figure 1 shows a screen shot of an analysis map as depicted in the WWS. Individual inputs such as buoys, ships, CMAN stations, scatterometer winds and tropical model output are shown as color coded wind barbs.

In the AES40, many digitized storm analyses were brought in as kinematic fields for inclusion. These

storms were hindcast in previous projects and included such storms as the October 1991 “Halloween Storm”, March 1993 “Storm of the Century”, and other important storms. These storms had been hand-drawn as isotachs and streamlines and then tediously hand-gridded, typically on a ½ degree resolution. Two artifacts of this gridding process were in the degree of accuracy in areas of strong gradients and in the blending of the new wind field into the full basin winds. The inclusion of direct kinematic analysis within the WWS allowed these analyses to be brought into the basin wind fields with improved accuracy and with better blending into the full synoptic field. Archives of hand-drawn maps were restored from their original storm packets and placed on a digitizing tablet to be traced directly into the WWS. Figure 2 shows a sample analysis of isotachs and streamlines from the “Halloween” storm of October 1991. In areas with direct kinematics the drawn isotachs and/or streamline (the program allows either or both) are run through a separate objective analysis and overlaid on the final wind field. Winds along the boundary of the kinematic area are blended with winds from the objective analysis of the insitu and model data which ensures a good blend between the fields.

## 2.2 Wave Models

The wave model applied in the MSC50 was the same third generation wave model (OWI-3G) as used in the original AES40. However, advances in computer power now allowed the basin wide North Atlantic to be run at higher resolution of 0.5-degree and allowed the inclusion of shallow water effects.

Computational details on the OWI’s 3<sup>rd</sup> generation physics can be found in Khandekar *et al.* (1994) and Forristall and Greenwood (1998). Briefly, the energy balance equation may be written first in simplified form for deep water and no currents as follows:

$$\partial E / \partial t + \nabla \cdot (C_g E) = S \equiv S_{in} + S_{nl} + S_{ds}$$

where E, the directional wave spectrum, E (f,θ,x,t), is a function of wave frequency, f, wave direction, θ, position, x, and time, t, C<sub>g</sub> is group velocity and S represents the processes which grow and dissipate energy, the so-called source terms which are described further below. OWI3G follows rather faithfully the formulation of the first 3G spectral wave model, WAM (WAMDI, 1988) with a few notable exceptions as noted below.

### 2.2.1 The Spectral Resolution

Direction: 24 bands. Band 1 is centered 7.5° clockwise from true north, the width of each band is 15°

Frequency: Band 1 is centered on 0.039 hz; the bands increase in geometric progression (ratio = 1.10064) to band 23, .32157 hz. This binning is negligibly coarser than used WAMDI (ratio = 1.100) and no coarser than that used in typical 15 frequency binning of ODGP.

### 2.2.2 Propagation Scheme

The downstream interpolation scheme described by Greenwood *et al.* (1985) is used throughout. Propagation over a time step at a grid point is implemented within the alternate growth-propagation cycle in the model integration by forming linear combinations of spectral variances at neighboring points. The weights used are extracted from a precomputed table of propagation coefficients, which vary by latitude only in deep water, and are specific to each grid point in shallow water. The table of interpolation coefficients is calculated based upon great circle wave ray paths in deep water; in shallow water the weights are calculated following a ray tracing study through a digital bathymetry resolved on the wave model grid.

The limiting water depth for shallow propagation and growth processes is taken according to the conventional definition:

$kd > \pi$ , where  $k = .006123 \text{ m}^{-1}$  for the .039 hz frequency bin.

### 2.2.3 Spectral Growth/Dissipation Algorithms

As noted above, the theoretical basis of the spectral growth algorithm used in OWI3G follows closely that of WAM. In WAM, separate source terms for the physical mechanisms of atmospheric input, S<sub>in</sub>, wave-wave interaction, S<sub>nl</sub>, and dissipation by whitecapping, S<sub>ds</sub>, (and in shallow water dissipation by bottom friction, S<sub>b</sub>) are specified explicitly and the source term balance is integrated to yield the net development of the spectrum over a time step of integration without arbitrarily forcing of spectral shape or specification of an external limit to growth. However, in the original development of the model, considerable experimentation with and tuning of the input and dissipation source terms was carried out (Komen *et al.*, 1985) to achieve growth rates and asymptotic behavior under constant winds in agreement with field data. The wave-wave interaction "apparent" source term, S<sub>nl</sub>, is not considered tunable and is a parameterization of the exact nonlinear interactions as proposed (see *e.g.* Hasselmann and Hasselmann, 1985). This so-called

Discrete Interaction Approximation (DIA) is also described in WAMDI (1988).

OWI3G combines a source term representation and integration scheme based upon WAM with the propagation scheme described above. The source terms follows the theoretical forms used in WAM but with different numerics and code and with the following modifications. First, a linear excitation source term is added to  $S_{in}$ , taken as a downscaled variant of the term used in OWI's 1G ODGP model (see e.g. Khandekar et al., 1994 for a description of the 1G model source terms). This allows the sea to grow from a flat calm initial condition in OWI3G, unlike all cycles of WAM which require an artificial warm start from a prescribed initial spectrum. The exponential input term is the empirical form of Snyder et al. (1981) in which  $S_{in}$  is taken as a linear function of friction velocity  $U_*$ . However, unlike WAM in which  $U_*$  is computed from the 10 meter wind speed  $U_{10}$  following the drag law of Wu (1982), in OWI3G, a different drag law is used that was developed in the model tuning stage. That drag law follows Wu closely up to about 20 m/sec then becomes asymptotic to a constant at wind speeds above 30 m/s. It appears that OWI3G was the first wave model to incorporate a saturation surface drag formulation. That is, rather than retain the usual unlimited linear increase of the drag coefficient with increasing wind speed, OWI3G capped the drag coefficient at a value of  $2.2 \times 10^{-3}$  at a wind speed of about 30 m/s. Recent estimates of the 10-m surface marine drag coefficient in extreme winds in the field (Powell et al., 2003) and in a wind-tunnel/wave-tank set up (Donelan et al., 2005) tend to support the notion of saturation of the drag coefficient at high wind speeds.

The non-linear term is approximated by the standard DIA except that in OWI's model a second quartet of interactions is included as described by Forristall and Greenwood (1998). As in WAM, the non-linear transfer for waves in shallow water are described by the deep water transfer multiplied by a scaling factor which is a function of wave number and water depth.

The dissipation source term,  $S_{ds}$  is also taken from WAM except that the dependence on frequency is cubic rather than quadratic.

OWI3G was developed based upon tuning runs against the fetch-limited growth benchmark for 20 m/s wind speeds under constant winds used to tune WAM, and trial hindcasts of a well-documented moderate extratropical cyclone (SWADE IOP-1, see Cardone et al., 1995) and two intense Gulf of Mexico hurricanes (Camille, 1969; Frederick, 1979). The bottom friction

source term is a simple quadratic law with a specified tunable friction factor. OWI3G uses the same friction factor found in the North Sea version of WAM (NEDWAM) to yield skillful shallow water predictions. That factor, .076, is exactly twice the value originally proposed for WAM, which was based upon studies of pure swell attenuation in the North Sea JONSWAP experiment.

An interesting comparison of the performance of OWI's first generation (1G) model and OWI3G in an extratropical setting is given by Khandekar, et al. (1994). A comparison of the performance of OWI1G, OWI3G and the latest cycle of WAM (WAM-4) in extreme storms is given in Cardone et al. (1996). Both of these studies as well as several unpublished studies, indicate that the differences in skill between OWI1G and OWI3G, at least for an integrated property of the spectrum such as HS or TS, are very slight and subtle despite the large differences in model formulation and computing requirements. Much more extensive validations of OWI's 3G wave model in long-term hindcast studies are given recently by Swail and Cox (2000) and Cox and Swail (2001).

#### 2.2.4 MSC50 Implementation of OWI-3G

Figure 3 shows the MSC30 basin wide model grid. Like the AES40, boundary spectra along the equator were supplied from the GROW (Global Reanalysis of Ocean Waves) hindcast which applied a 2<sup>nd</sup> generation wave model on a global grid (Cox and Swail, 2001). Inscribed in the MSC30S model grid is the fine domain MSC06Min 0.1-degree shallow water implementation of the OWI-3G model (Figure 4). This regional grid represents 18551 active grid points; this is more than twice the original AES40 which covered the entire North Atlantic.

Bathymetry for the MSC30S basin and MSC06Min model were supplied from two basic sources. The GEBCO (General Bathymetric Chart of the Oceans) digital atlas (2003 edition) provided water depths for most of the basin wide hindcasting. This source data is a gridded product with resolution of 1-minute covering the global oceans. Depths for the MSC06Min grid as well as overlapping regions of the MSC30S grid were supplied from the Canadian Hydrographic Service 15-second archive.

### 2.3 Ice Edge

In the OWI-3G model grid point locations with greater than 50% ice concentration are considered as land with no wave generation and/or propagation. In the AES40 the model required specification of the ice edge at the

start of each monthly segment for run. Mean monthly ice concentration data were applied from the Walsh and Johnson (1979), SIGRID (Gridded Ice Information), GFSC (Goddard Space Flight Center) and DSMP (Defense Meteorological Satellite Programs) sources all obtained from the National Snow and Ice Data Center. In the MSC50, the ice edge was allowed to change on a weekly basis. This allowed the MSC50 hindcast to better represent the changing ice conditions during the transition periods. In Canadian waters, the Canadian Ice Service (CIS) supplied two high-resolution ice concentration datasets that spanned the period 1962 to present (Table 1). Since these sources were weekly, the time period of all ice data were binned and averaged to the CIS times. Thus, the MSC30S basin model which covers the entire North Atlantic would apply the CIS data in Canadian waters and transition to the globally available sources in the rest of the model domain. Prior to 1962 only the mid-monthly Walsh and Johnson dataset was available. Figure 5 shows a comparison of the ice edge analysis during the CIS period (bottom) and Walsh and Johnson (top) during February of two different years. The Walsh and Johnson dataset is much coarser in resolution than the CIS data. It should be noted that no ice exists in the Gulf of St. Lawrence prior to 1962 since this is not included in the Walsh and Johnson grids. All grid points in the Gulf of St. Lawrence were treated as open sea (no ice) for the 1954-1961 period.

**Table 1 Ice concentration data sources**

Source	Frequency	Coverage	Date Range
Walsh and Johnson	Monthly	Full	Jan 1954-Dec 1971
SIGRID	Weekly	Full	Jan 1972-Oct 1978
GFSC	Daily	Full	Nov 1978-Dec 2000
DMSP	Daily	Full	Jan 2001-Present
CIS Gridpoint	Weekly	Canadian Waters	Jan 1962-Jul 1983
CIS NetCDF	Weekly	Canadian Waters	Jan 1971-Present

### 3. VALIDATION

#### 3.1 Validation Data Sets

##### 3.1.1. Buoys and Platforms

The *in situ* validation data set included buoys and measurement platforms mainly located along the continental margins. The *in situ* measured wind and wave data came from a variety of sources. U.S. buoy data came from the NOAA Marine Environmental Buoy Database on CD-ROM; the Canadian buoy data came from the Marine Environmental Data Service (MEDS) marine CD-ROM; the remaining buoy and platform data (notably the northeast Atlantic) came from the International Comprehensive Ocean Atmosphere Data Set (ICOADS) data set described by Worley *et al.* (2006). Comparisons were restricted to well-exposed sites (as determined by the model resolution being compared) with the longest records. The wave measurements are comprised of 20-minute samples (except for Canadian buoys which were 40 minutes) once per hour. The wind measurements were taken as 10-minute samples, scalar averaged, except vector averaged at the Canadian buoys prior to 1998, also once per hour. The wind and wave values selected for comparison with the hindcast were 3-hour mean values centered on each six-hour synoptic time with equal (1,1,1) weighting. All wind speeds were adjusted to 10-m neutral winds following the approach described in Cardone *et al.* (1990).

##### 3.1.2. Satellite Data

Altimeters from the ERS-1, ERS-2 and TOPEX/Poseidon instruments were used for wind and wave comparisons. The ERS-1/2 altimeter data sets were obtained from the Ifremer CD-ROM data set, while TOPEX data (GDR Generation-B CD-ROM set) were obtained from the NASA Physical Oceanography Distributed Active Archive Center at the Jet Propulsion Laboratory/California Institute of Technology. Both data sets were decoded using the recommended quality controls described in each respective documentation. Further adjustments and quality control measures were used as recommended by Cotton and Carter (1994) to make the observations from differing platforms consistent with each other. Individual data points were then spatially binned onto the 0.5-degree MSC30S wave model grid, and output on to 1-hour synoptic times using a  $\pm 30$ -minute window. Additional quality control was performed for measurements along land and ice edges where some contamination of the altimeter wave measurements was encountered despite rigorous checking of ice/quality control flags available with each data set.

### 3.2 *In situ* Comparisons

Individual buoys and platforms were grouped by region for comparison against the MSC30S region hindcast. Table 2 shows regional grouped statistics and represents more than 2,000,000 wind and wave observations. Highest scatter indices (SI) are from the northeast Atlantic regions, which were made up exclusively of ICOADS data. The ICOADS data lacks both the time resolution (3/6 hours versus 1 hour) and

coding accuracy (winds nearest 1 knot, waves 0.5 m) than the other regions obtained from the CD-ROM marine data sets, which may explain some of the differences in SI. The Canadian and U.S. buoys were grouped into one data set since they represented the best science quality validation data set. These statistics show very good agreement with a mean bias of 0.01 m/s for winds (0.31 in AES40) and 0.08 m for waves (0.10 for AES40) and SI of 0.08 for winds (0.23 in AES40) and 0.16 for waves (0.23 in AES40).

Table 2. Regional statistical comparison of MSC30S basin hindcast vs. *in situ* buoy and platform observations.

	<b>Number of Points</b>	<b>Mean Meas</b>	<b>Mean Hind</b>	<b>Diff (H-M)</b>	<b>RMS Error</b>	<b>Std. Dev.</b>	<b>Scatter Index</b>	<b>Corr. Coeff.</b>
<b><i>U.S. and Canadian Buoys</i></b>								
<b>Ws (m/s)</b>	1892276	7.09	7.10	0.01	0.60	0.60	0.09	0.99
<b>Wd (°)</b>	1863466	248.27	249.63	0.28	N/A	7.57	0.02	N/A
<b>Hs (m)</b>	1925965	1.70	1.79	0.08	0.28	0.27	0.16	0.96
<b>Period (s)</b>	1879419	5.98	5.69	-0.29	0.58	0.50	0.08	0.96
<b>VMD(°)</b>	241169	127.86	139.10	9.17	N/A	23.76	0.07	N/A
<b><i>Eastern Atlantic / North Sea /Norwegian Sea Platforms and Buoys</i></b>								
<b>Ws (m/s)</b>	942960	8.37	8.52	0.15	0.93	0.92	0.11	0.97
<b>Wd (°)</b>	943544	237.23	237.05	-0.66	N/A	8.75	0.02	N/A
<b>Hs (m)</b>	386291	2.48	2.71	0.23	0.53	0.47	0.19	0.95
<b>Period (s)</b>	392170	10.06	9.19	-0.87	3.57	3.46	0.34	0.42
<b><i>All Data Combined</i></b>								
<b>Ws (m/s)</b>	2827968	7.49	7.54	0.05	0.71	0.71	0.09	0.98
<b>Wd (°)</b>	2806995	242.94	243.61	-0.02	N/A	8.00	0.02	N/A
<b>Hs (m)</b>	2316795	1.83	1.93	0.10	0.32	0.30	0.17	0.96
<b>Period (s)</b>	2168226	6.37	6.10	-0.27	0.93	0.89	0.14	0.91
<b>VMD(°)</b>	241169	127.86	139.10	9.17	N/A	23.76	0.07	N/A

Table 3. Regional statistical comparison of MSC06Min region hindcast vs. *in situ* buoy and platform observations.

	<b>Number of Points</b>	<b>Mean Meas</b>	<b>Mean Hind</b>	<b>Diff (H-M)</b>	<b>RMS Error</b>	<b>Std. Dev.</b>	<b>Scatter Index</b>	<b>Corr. Coeff.</b>
<b><i>Buoys with Depths &lt; 50 meters</i></b>								
<b>Ws (m/s)</b>	208011	6.29	6.28	-0.01	0.46	0.46	0.07	0.99
<b>Wd (°)</b>	204717	254.32	254.92	0.75	N/A	6.56	0.02	N/A
<b>Hs (m)</b>	282913	1.05	1.12	0.07	0.27	0.26	0.25	0.95
<b>Period (s)</b>	274143	5.68	5.34	-0.35	0.90	0.84	0.15	0.91
<b>VMD(°)</b>	26385	84.31	89.11	7.48	N/A	20.18	0.06	N/A
<b><i>All Data Combined</i></b>								
<b>Ws (m/s)</b>	951814	6.99	7.04	0.04	0.69	0.69	0.10	0.98
<b>Wd (°)</b>	947891	259.50	260.48	0.41	N/A	8.62	0.02	N/A
<b>Hs (m)</b>	1271451	1.72	1.80	0.08	0.32	0.31	0.18	0.96
<b>Period (s)</b>	1249378	7.09	6.81	-0.28	0.89	0.85	0.12	0.94
<b>VMD(°)</b>	26385	84.31	89.11	7.48	N/A	20.18	0.06	N/A

In the MSC06Min regional model, only data from the U.S. Buoy and Canadian MEDS data were available for comparison. The Canadian dataset included MEDS and WEL wave-only data archived by MEDS which primarily consisted of wave measurements in transitional and shallow water depths. Figure 6 shows all the validation locations for sites within the 0.1 degree model grid. Depths range from 19.5 meters (MEDS152) to 4,527 meters (Buoy 44141). Table 1 shows the statistical comparisons for locations less than 50 meters water depth and all locations. There are over 1,200,000 wave measurements and just under 1,000,000 wind measurements since not all measurement platforms report winds. Overall the winds and wave show excellent agreement with 0.04/0.10 bias/SI for winds and 0.08/0.18 bias/SI for waves. The statistical comparisons are comparable for the locations in depths less than 50 meters.

A quantile-quantile comparison of wind speed and wave height for the combined buoys is shown for the MSC30S basin (Figure 7) and MSC06Min region (Figure 8). Both show excellent agreement from the 1<sup>st</sup> to 99<sup>th</sup> percentiles (blue) and even in the most extreme storms represented by the 99.1 to 99.9 percentiles (red).

While overall statistics are useful for evaluating the skill of a hindcast, they don't indicate how the hindcast has changed over time relative to the *in situ* data. A comparison of yearly wave height bias and scatter over the 1978-2005 period (MSC30S Figure 9, MSC06Min Figure 10) shows any trends that may exist in the hindcasts. Of course, trends may also occur in the measurements themselves (number of observations available, differing instrumentation, etc.) and the

measured data must be evaluated carefully. These plots were produced by computing bias every 1 year and plotting the resulting time series. The figures show good agreement between the buoy observations and MSC50 hindcast over time. The plots show nearly linear bias and SI over time indicating that MSC50 has remained consistent over the 28 years that the buoy measurements are available.

### 3.3 Satellite Comparisons

Altimeter wind and wave measurements provide the best spatial coverage to evaluate the MSC30S basin wave hindcasts. Statistics and plots from the individual instruments (ERS-1, ERS-2, and TOPEX) showed very good agreement between each other, so the data sets were combined for these comparisons. Comparisons were done for the full basin only. Statistics are summarized in Table 4. The wave height comparisons showed near-zero bias, while the model winds were slightly higher than the satellite values. Scatter indices were of comparable magnitude to the *in situ* comparisons.

Quantile-quantile (Q-Q) plots of the combined altimeter versus MSC30S (Figure 11) show excellent agreement for both wind speed and wave height. At the highest percentiles, winds appear to be over-predicted while waves track up to the 99<sup>th</sup> percentile. This is suspected to be a wind speed saturation problem with the altimeter in wind speeds above 15 m/s.

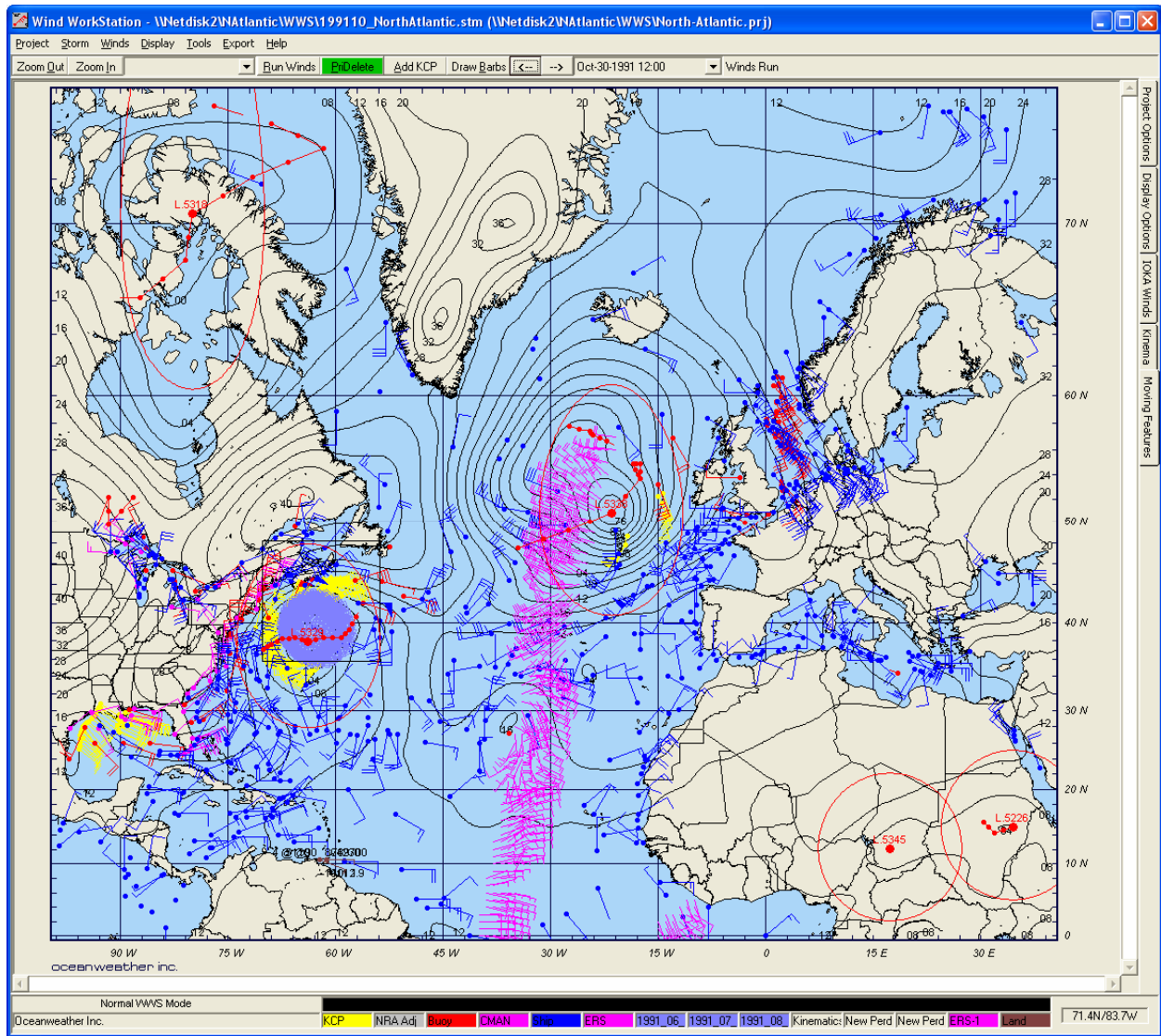


Figure 1. Screen shot of the Wind WorkStation valid October-30-1991 12:00 GMT.

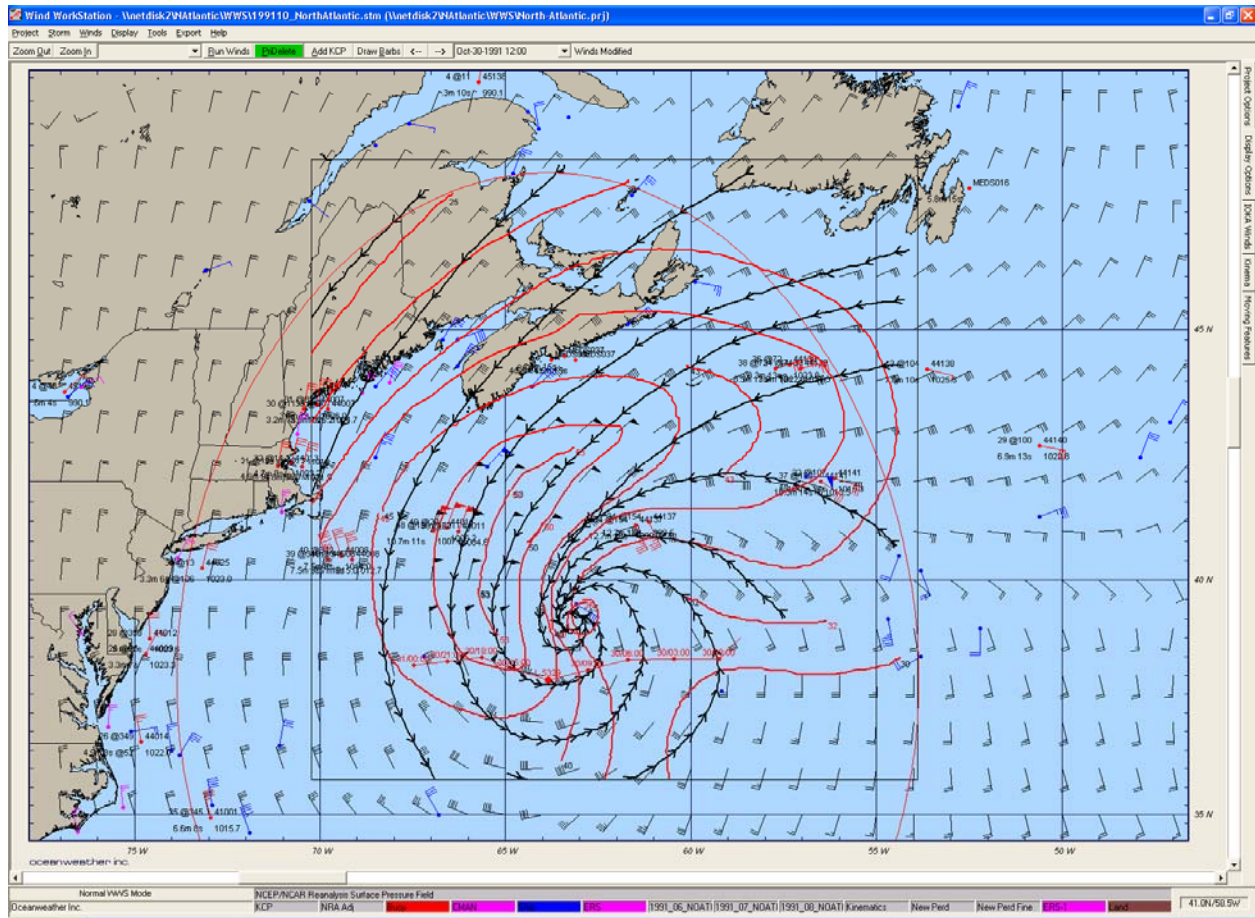


Figure 2. Example of hand-drawn isotachs (red) and streamlines (black) during “Halloween Storm” valid October 30, 1991 12:00 GMT.

MSC50 Wind and Wave Climatology  
MSC30S Shallow Water Wave Model Grid

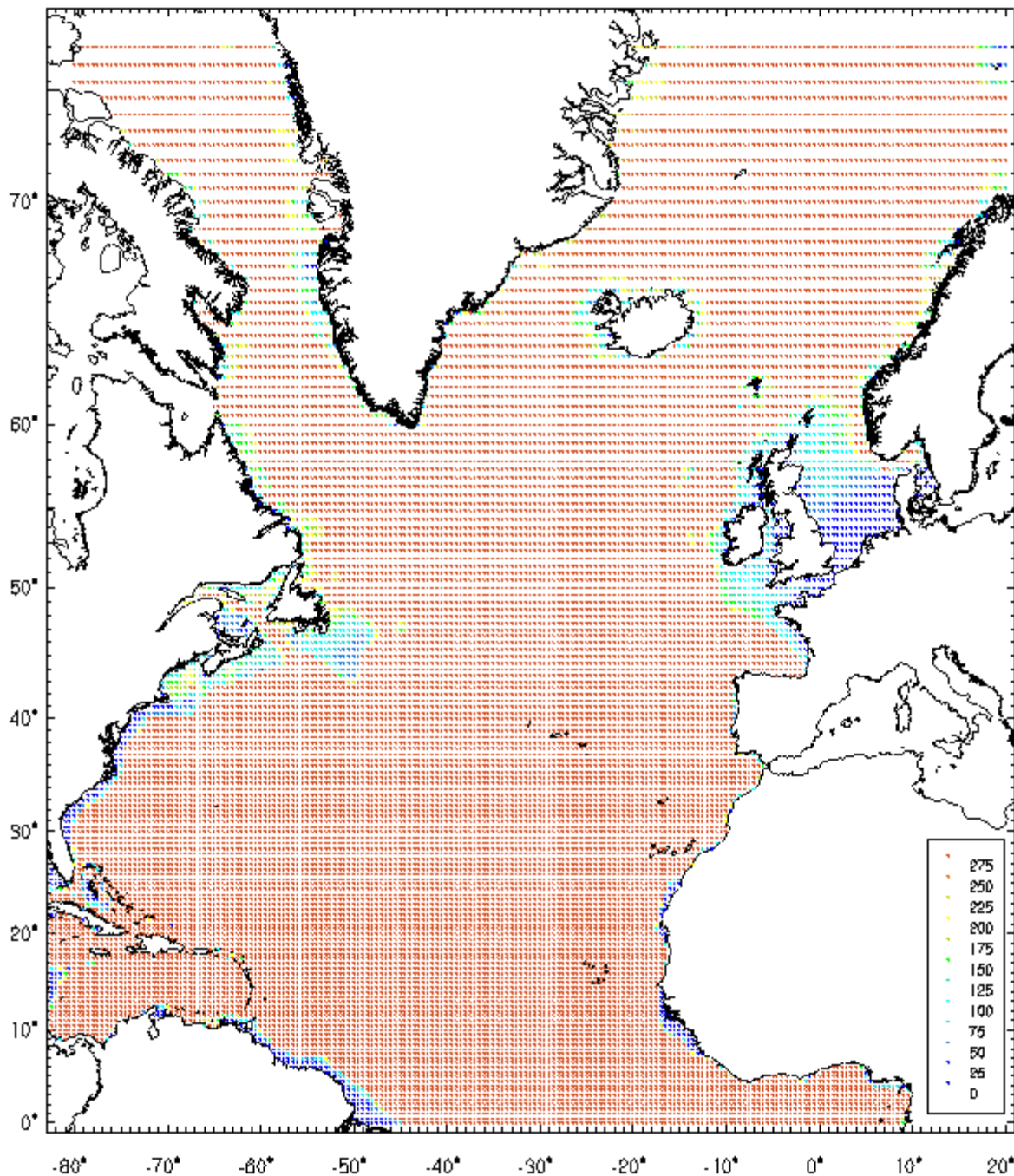


Figure 3. MSC30S basin wave model grid (0.5-degree resolution), color coded by depth (m)

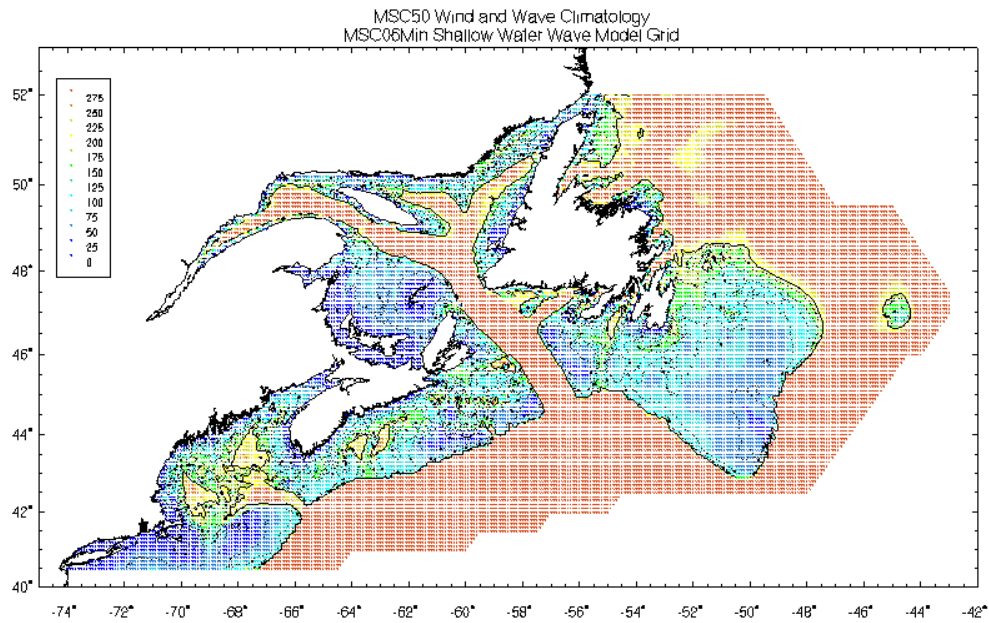


Figure 4. MSC06Min region wave model grid (0.1-degree resolution) , color coded by depth (m)

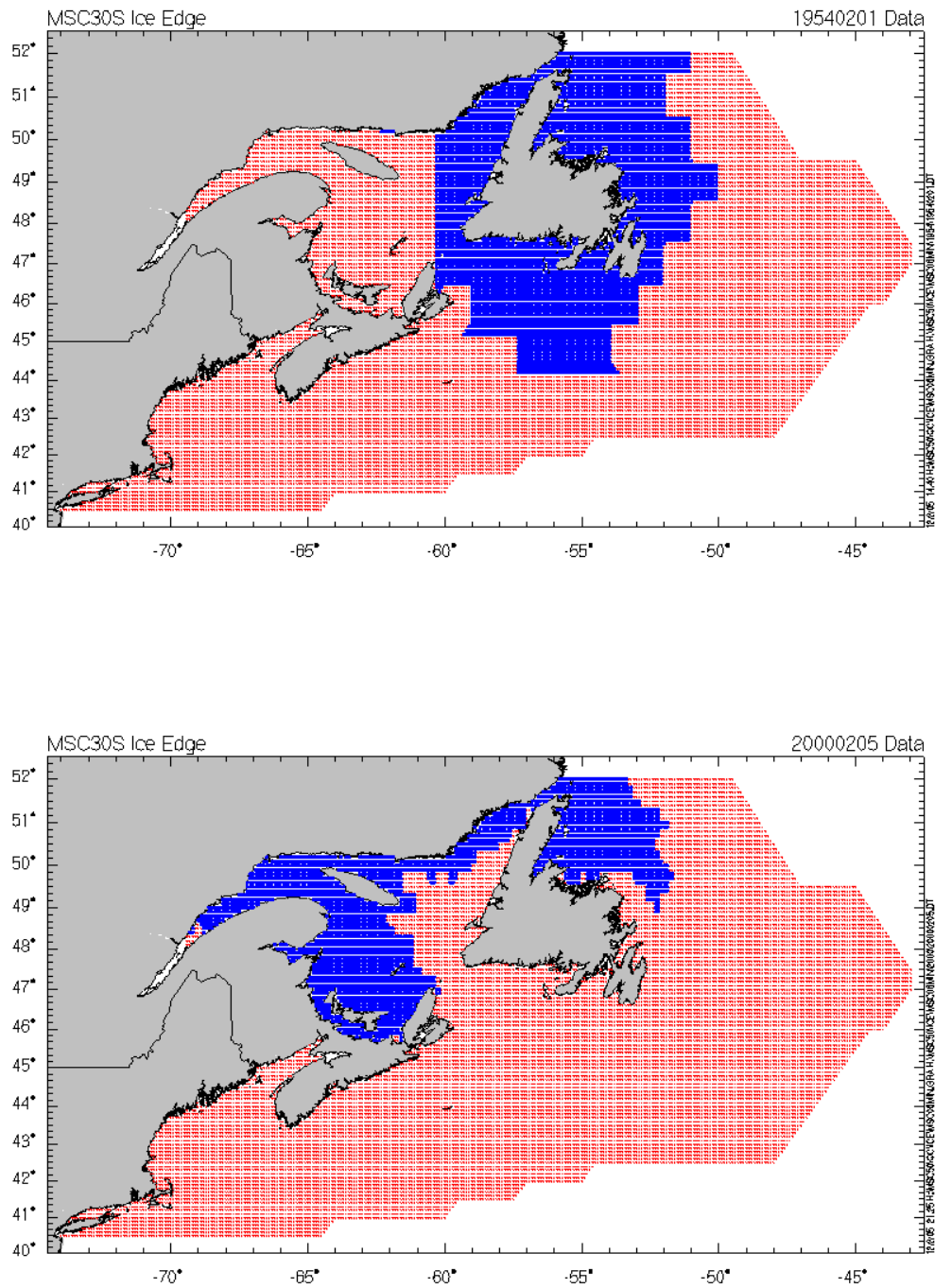


Figure 5. Comparison of mean monthly Walsh and Johnson ice edge (greater than 50% concentration) during February 1954 with weekly Canadian Ice Service ice edge during the first week of February 2000 on the MSC06Min regional grid.

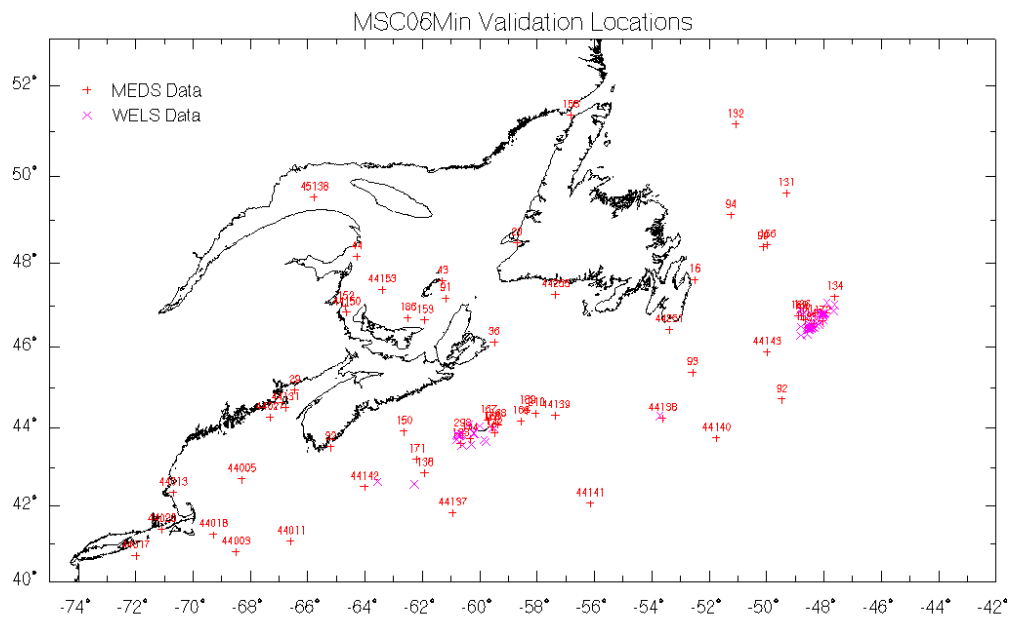


Figure 6. MSC06Min region wave model *insitu* validation locations

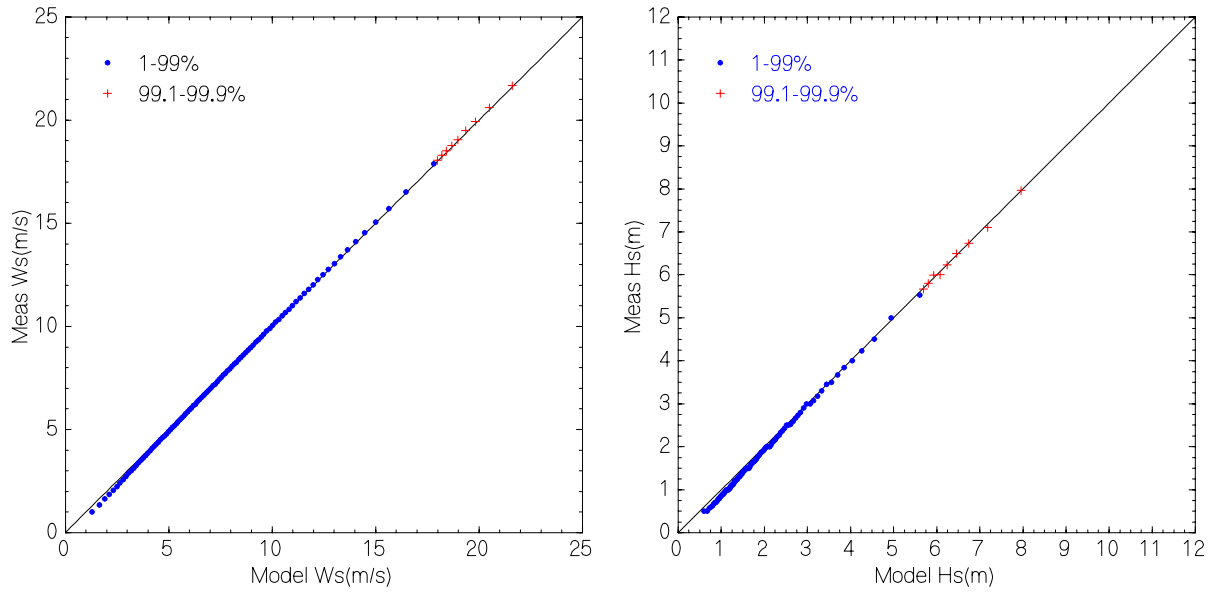


Figure 7. Quantile-Quantile comparison from 1 to 99% for combined *insitu* data vs. MSC30S basin hindcast wind speed (m/s, left) and significant wave height (meters, right).

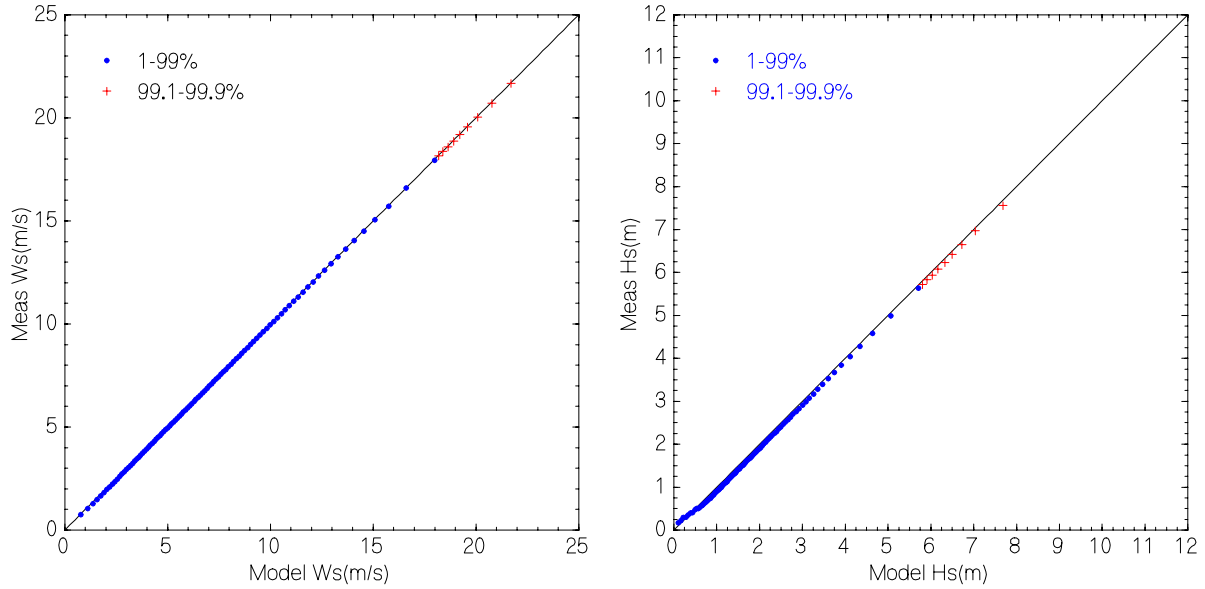


Figure 8. Quantile-Quantile comparison from 1 to 99% for combined *insitu* data vs. MSC06Min region hindcast wind speed (m/s, left) and significant wave height (meters, right).

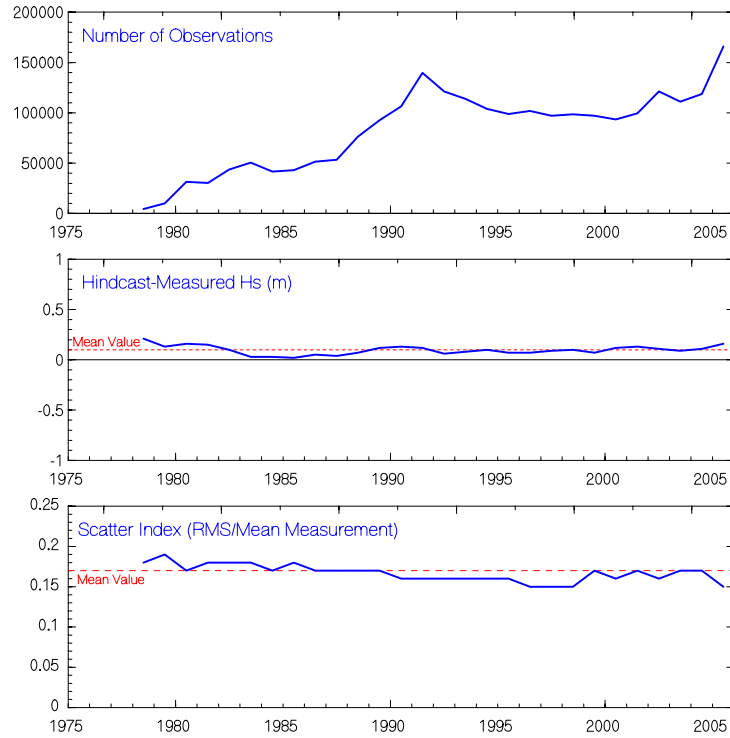


Figure 9. Comparison of number of *insitu* observations (top), MSC30S basin hindcast wave height bias (middle) and scatter index (bottom) computed monthly over the time period 1978-2005.

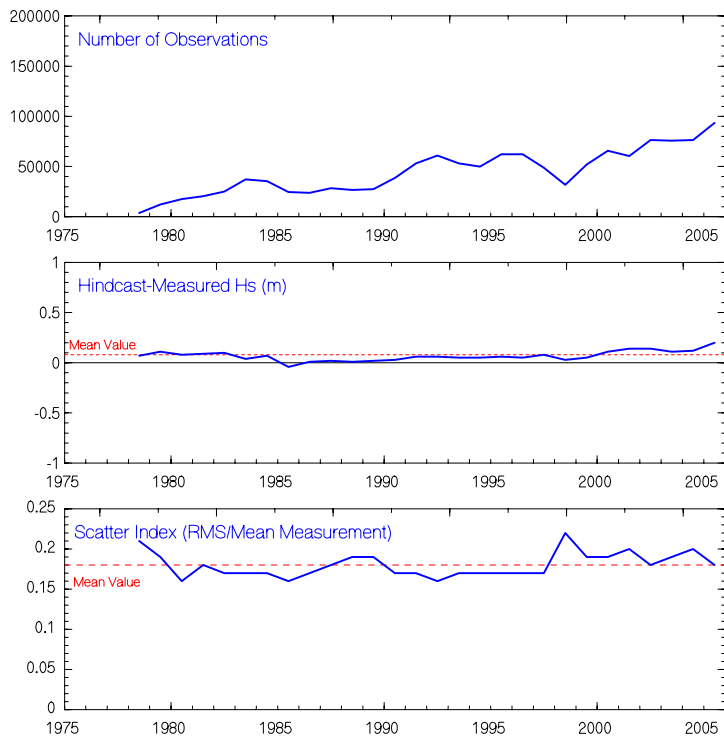


Figure 10. Comparison of number of *insitu* observations (top), MSC06Min region hindcast wave height bias (middle) and scatter index (bottom) computed monthly over the time period 1978-2005.

Table 4. Regional statistical comparison of MSC30S basin hindcast vs. altimeter measurements.

	Number of Points	Mean Meas	Mean Hind	Diff (H-M)	RMS Error	Std. Dev.	Scatter Index	Corr. Coeff.
Ws (m/s)	5063147	7.45	7.69	0.24	1.52	1.50	0.20	0.90
Hs (m)	5434181	2.43	2.47	0.04	0.40	0.40	0.17	0.95

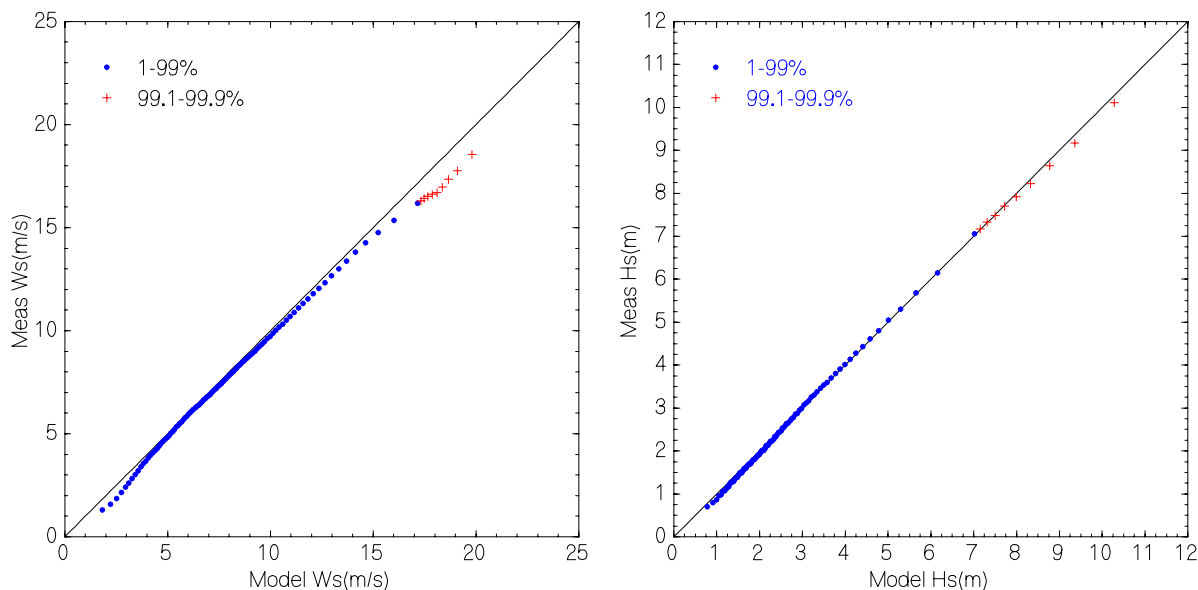


Figure 11. Quantile-Quantile wind speed (m/s) and wave height (m) comparisons of MSC30S basin hindcast and altimeter measurements from 1%-99% (blue, every 1%) and 99.1%-99.9% (red, every 0.1%)

The extensive coverage of the altimeter measurements makes it possible to plot contours of wave bias on a basin-wide projection. A spatial wave bias plot of MSC30S (Figure 12) shows that over most of the North Atlantic AES40 has very little bias. An area of underestimation in Baffin Bay and in the Denmark Strait noted in the original AES40 hindcast was attributed to ice edge effects caused by the mid-monthly ice edges. This underestimation has been largely eliminated in the MSC50 hindcast largely due to the inclusion of higher spatial and temporal ice edge data. Another area of improvement is in the Southern North Sea where inclusion of shallow water effects has greatly decreased the over-estimation found in the AES40 hindcast.

A basin map of wave height scatter index (SI) (Figure 13) shows many of the same patterns as the wave height bias map. In general, the SI is very small (near or under .20 for most of the basin) with larger values at the coasts and along water/ice boundaries.

#### 4. REANALYSIS DATA AND CLIMATE PRODUCTS

##### 4.1 Hindcast Data

Wind and wave fields from the MSC30S basin hindcast and MSC06Min region hindcast in Canadian waters were archived at a 3-hour and 1-hour time-step respectively (Figure 14). These fields were then point-sorted for all Canadian waters locations so that 1 grid point file contains all fields for the 1954-2005 time period. Wind and wave fields include wind speed, wind direction; significant wave height, peak period and vector mean direction of the total, sea partition and swell partition of the waves; as well as directional spreading parameters.

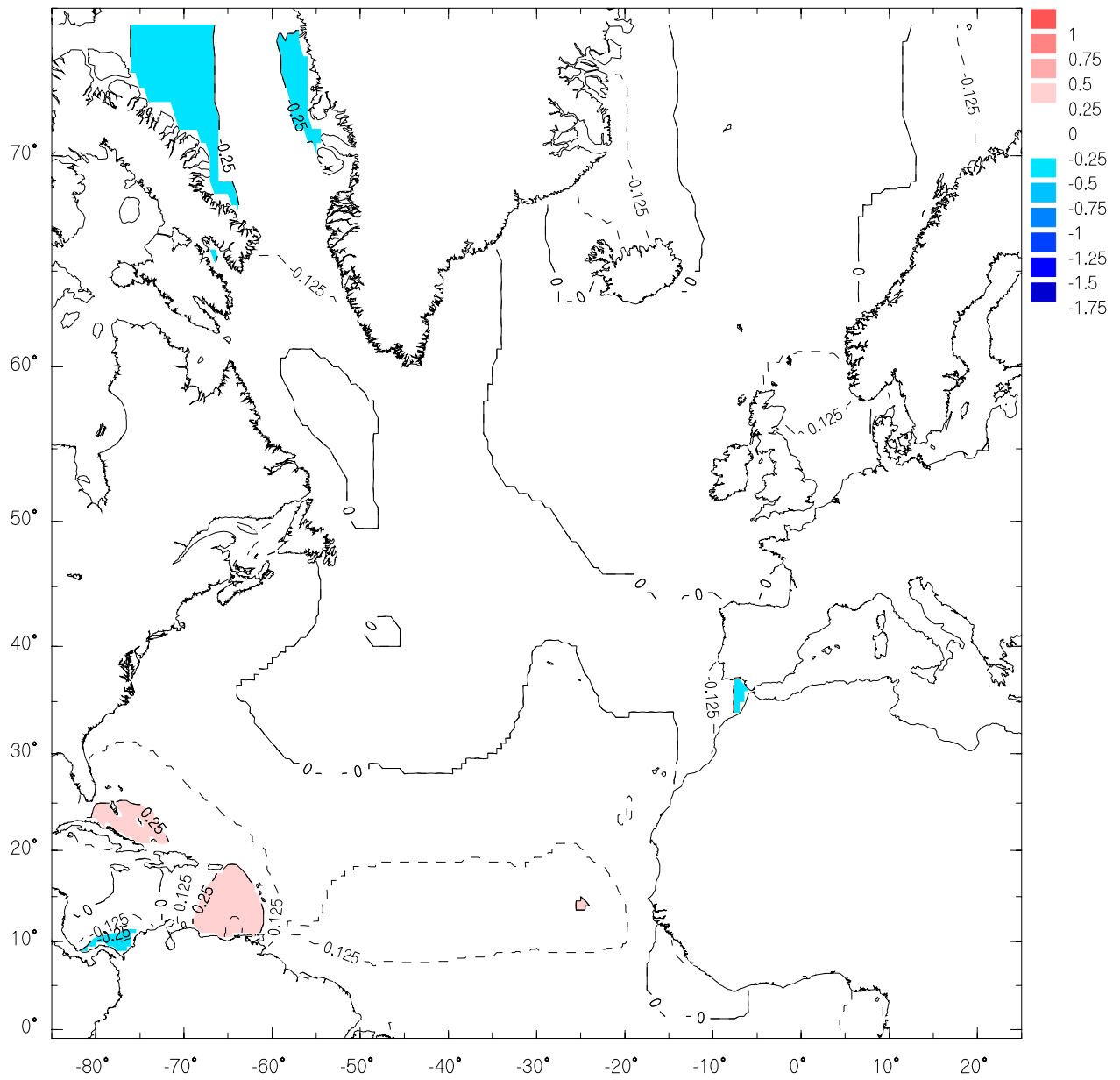


Figure 12. Mean difference of wave height (m) between MSC30S basin hindcast and altimeter measurements (MSC30S-Altimeter) for the period 1987-2005.

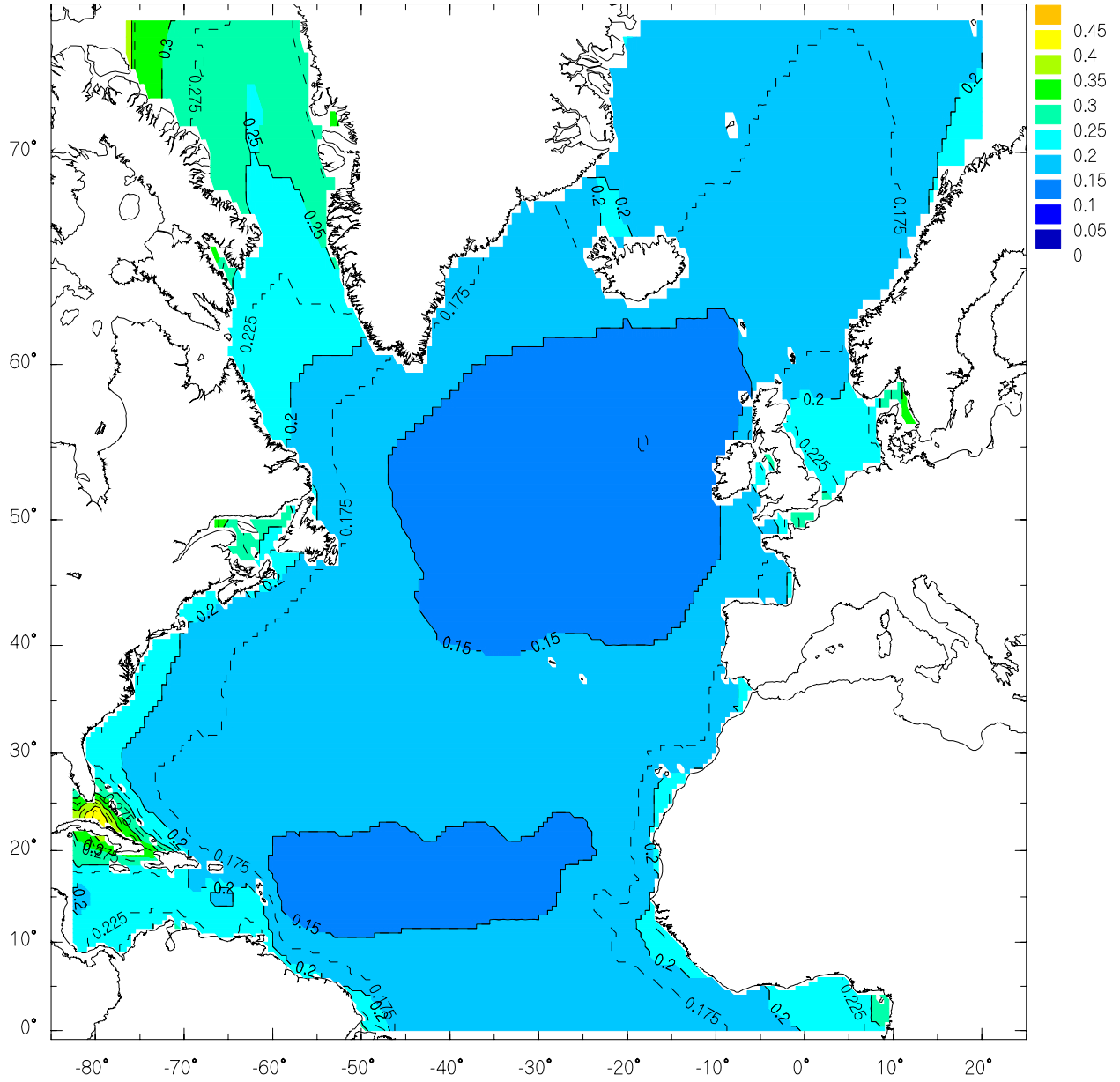


Figure 13. Comparison of wave height scatter index (RMS/Mean Altimeter) for combined altimeter wave measurements vs. MSC30S basin hindcast for the period 1987-2005.

Directional wave spectra from the hindcast were also archived at a subset of the MSC30S and MSC06Min grids in Canadian waters (Figure 14, black). The MSC30S archived wave spectra every 2.5 degrees while the MSC06Min archived points every 0.4 degrees in deep water and every 0.2-degrees in shallow/intermediate depths and along the coastline. Wave spectra are archived in point-sorted format and contain 23 frequency by 24 directional band resolution at the same time-step as the wind and wave fields.

#### 4.2 Climate Atlas

An online wind and wave atlas was produced for the entire MSC30S and MSC06Min domains; as well as the original AES40. The atlas can be viewed at <http://www.oceanweather.com/MS50WaveAtlas/>, a sample image is shown in Figure 19. This atlas includes mean, median, 90<sup>th</sup> percentile, 99<sup>th</sup> percentile, standard deviation, and 3 exceedence levels expressed graphically for both winds and waves. Anomalies from the 1954-2004 reference period are also shown for the mean, 90<sup>th</sup> and 99<sup>th</sup> percentiles. Results are time stratified for the entire period (1955-2004), all months, as well as individual months and individual years. A screen shot of the atlas is shown in Figure 15. Examples of selected analyses are detailed below.

Figure 16 shows the mean wind speed (top, left), 99<sup>th</sup> percentile wind speed (top, right) mean significant wave height (bottom, left) and 99<sup>th</sup> percentile significant wave height (bottom, right) from the period 1955-2004 for the MSC30S basin hindcast. The mean and 99<sup>th</sup> percentile wind speed results are very similar to the original AES40 hindcast winds. This result is not surprising since the same methodology was applied and the AES40 wind fields provided the base set of data for MSC50. The mean and 99<sup>th</sup> percentile wave heights for the MSC30S also shows a similar result to the AES40 hindcast. The two hindcasts applied similar models (OWI-3G, deep for AES40 shallow for MSC30S) and grid resolutions were very close (0.625x0.833 vs. 0.5 x0.5). The largest differences occur in areas where the MSC30S benefited from shallow water effects and areas where ice edge specification was improved.

Mean and 99<sup>th</sup> percentile comparisons on the MSC06Min region grid are shown in figures 17 and 18 respectively. Also shown in figure 19 is the exceedance of 11 m/s for winds (above) and 3 meters for waves (below) as a percentage of days. Each 1-hourly time step was counted as 1/24<sup>th</sup> of a day,

summed over the 1955-2004 time period, then expressed as a percentage of days.

#### 4.3 Extreme Value Analysis

A peaks over threshold analysis was performed using the 1954-2005 Canadian waters MSC06Min regional grid output. A peak is defined as any event that is greater than the minimum significant wave height threshold, and must be separated from any other peak by at least 48 hours. The threshold for a wave height peak was taken as ½ the maximum value at each grid point.

All peaks were processed using the Gumbel (Gumbel, 1958) extremal distribution at each individual grid point, no spatial smoothing was applied. Figure 20 shows the resulting 100-year return period for winds (above) and significant wave height (below). No limit was placed on the 100-year wave height in shallow water for this analysis, thus results in shallow water may exceed breaking criteria. Wind speed values vary from just under 25 m/s in some coastal locations to over 35 m/s at the most exposed locations. Wave heights show much more detail with maximum 100-year wave heights in excess of 17 meters.

A comparison of the wave height extremes at the Hibernia platform (46.8N, 48.6W) was performed using the AES40 and MSC50 hindcast (Figure 21). 100-year return values from the two hindcasts are within 5 cm (15.52 for AES40 vs. 15.47 for MSC50); however the width of the confidence limits has been decreased over 25% from 1.53 meters to 1.22 meters.

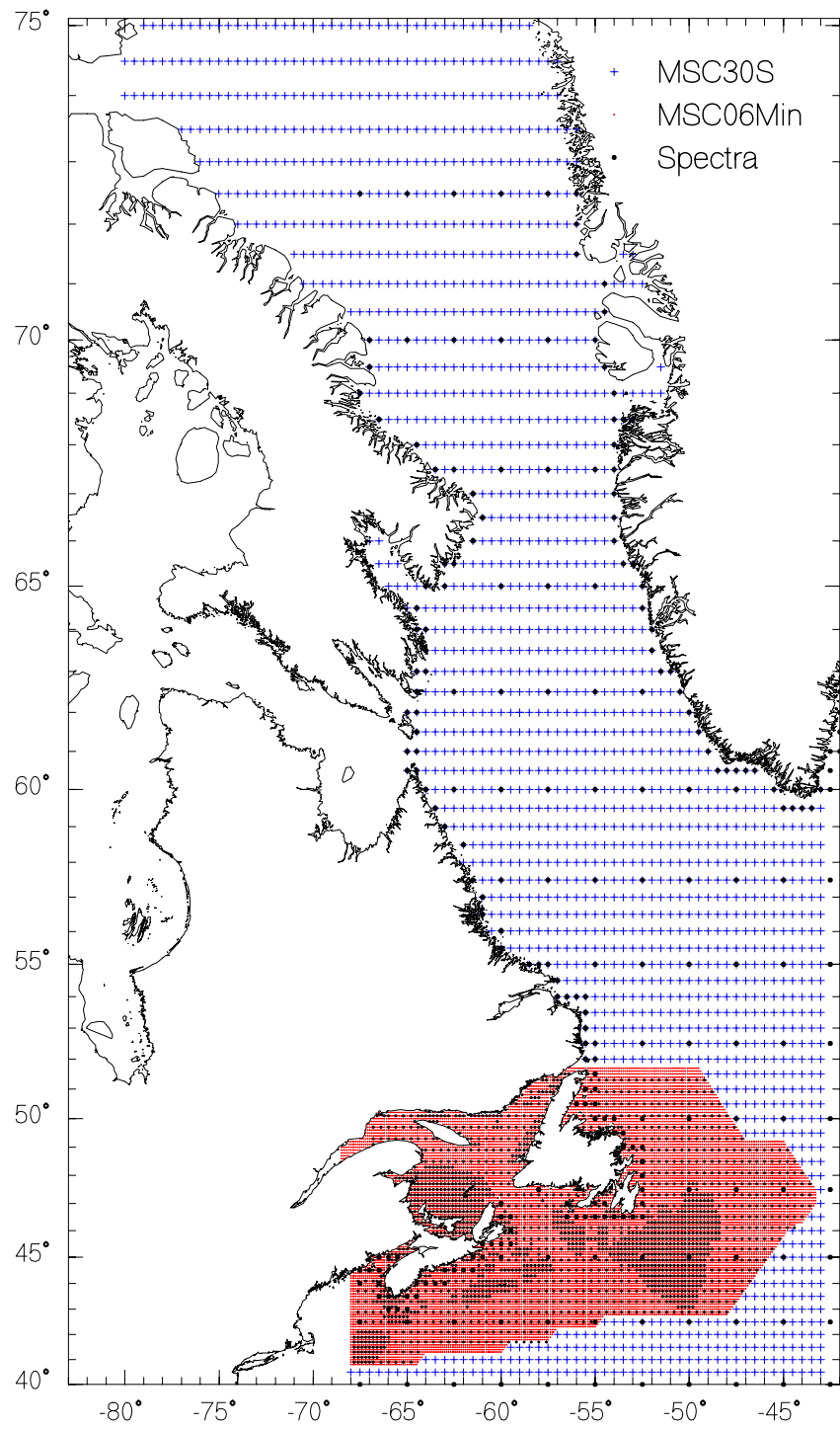


Figure 14. MSC50 archive locations of wind and wave fields (blue and red) and wave spectra (black)

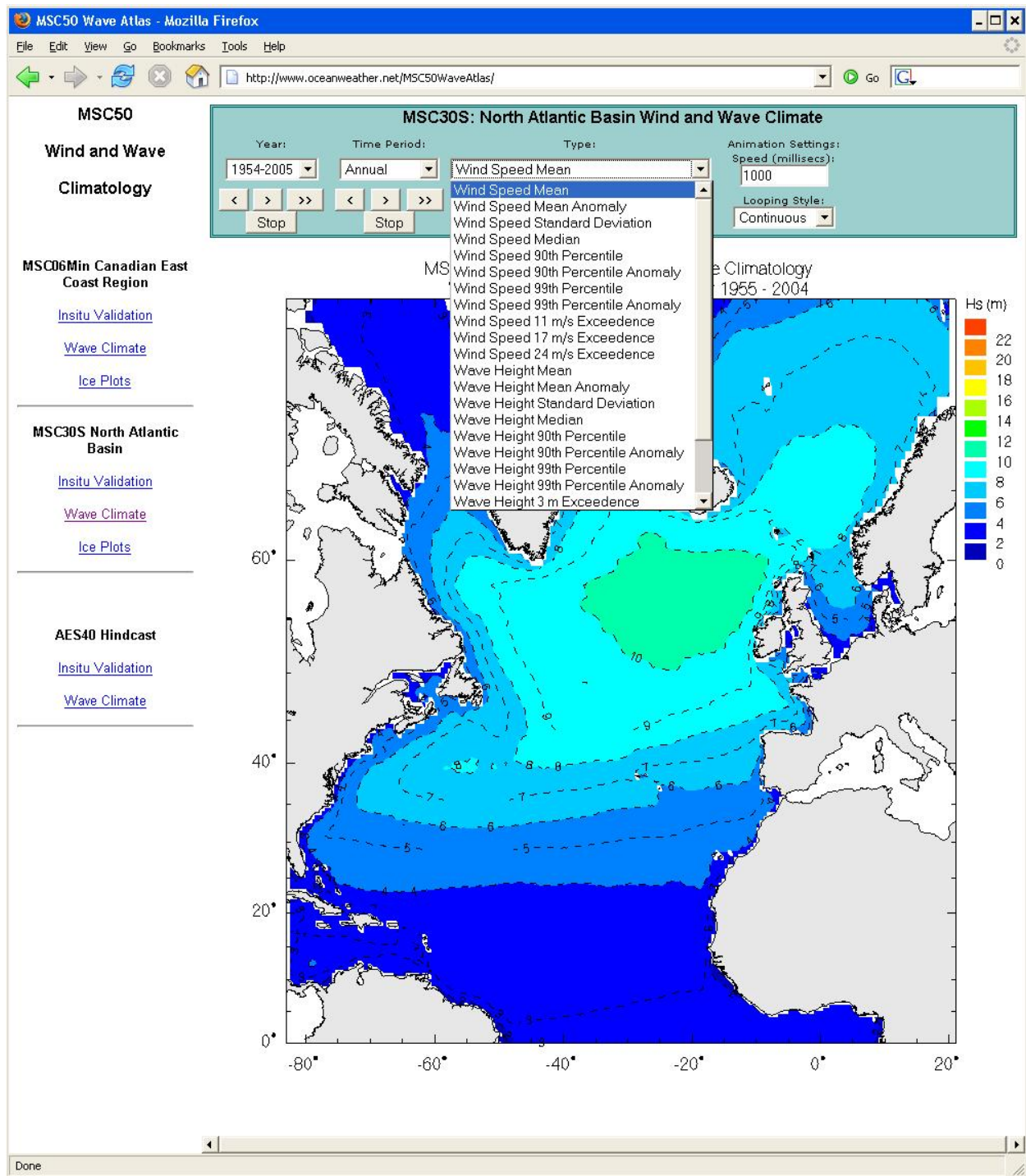


Figure 15. MSC50 Wave atlas online at <http://www.oceanweather.com/MSC50WaveAtlas/>

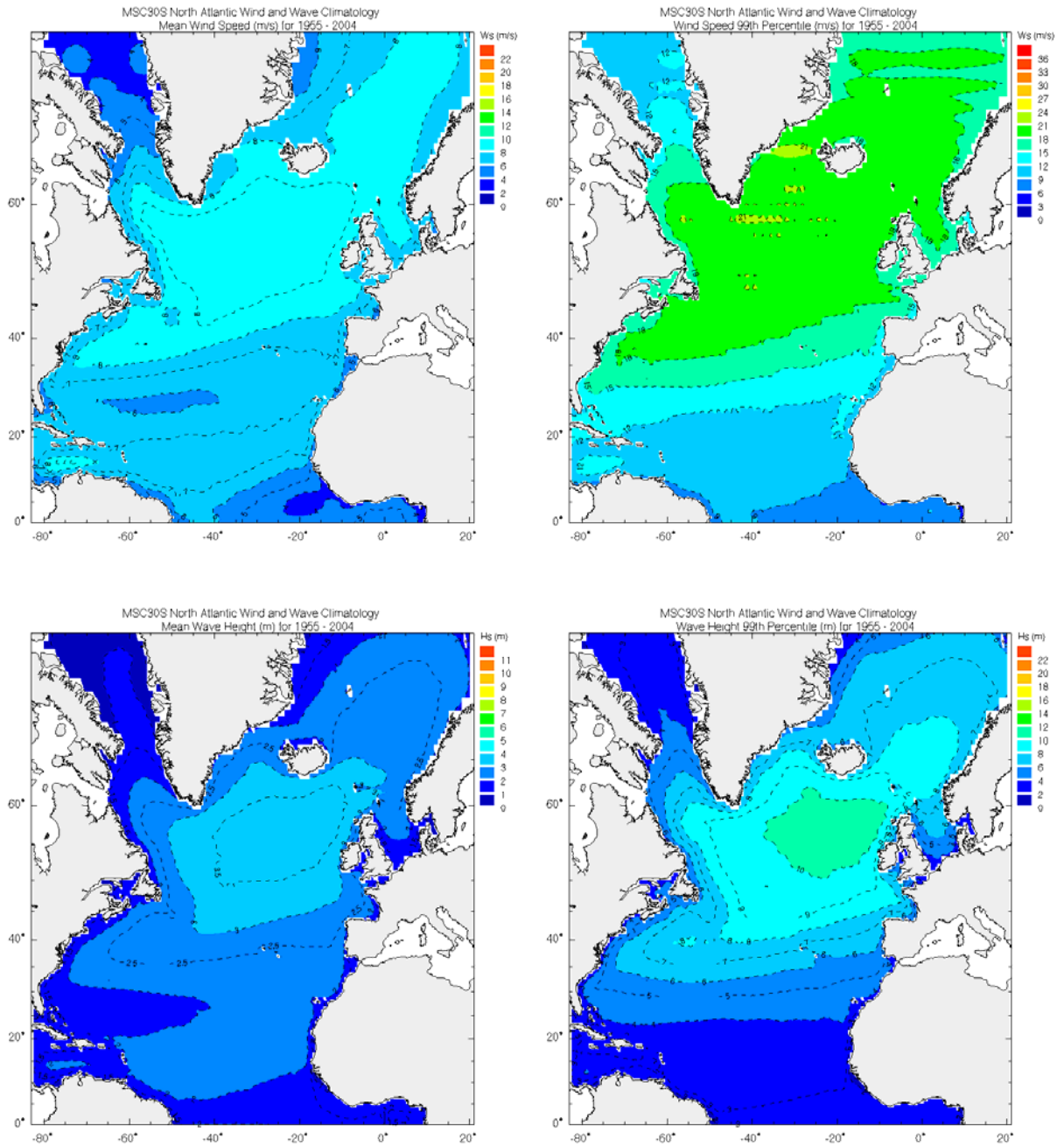


Figure 16. Wind speed and wave height statistics over the period 1955-2004: (a) annual mean wind speed; (b) 99<sup>th</sup> percentile wind speed; (c) annual mean wave height; (d) 99<sup>th</sup> percentile wave height

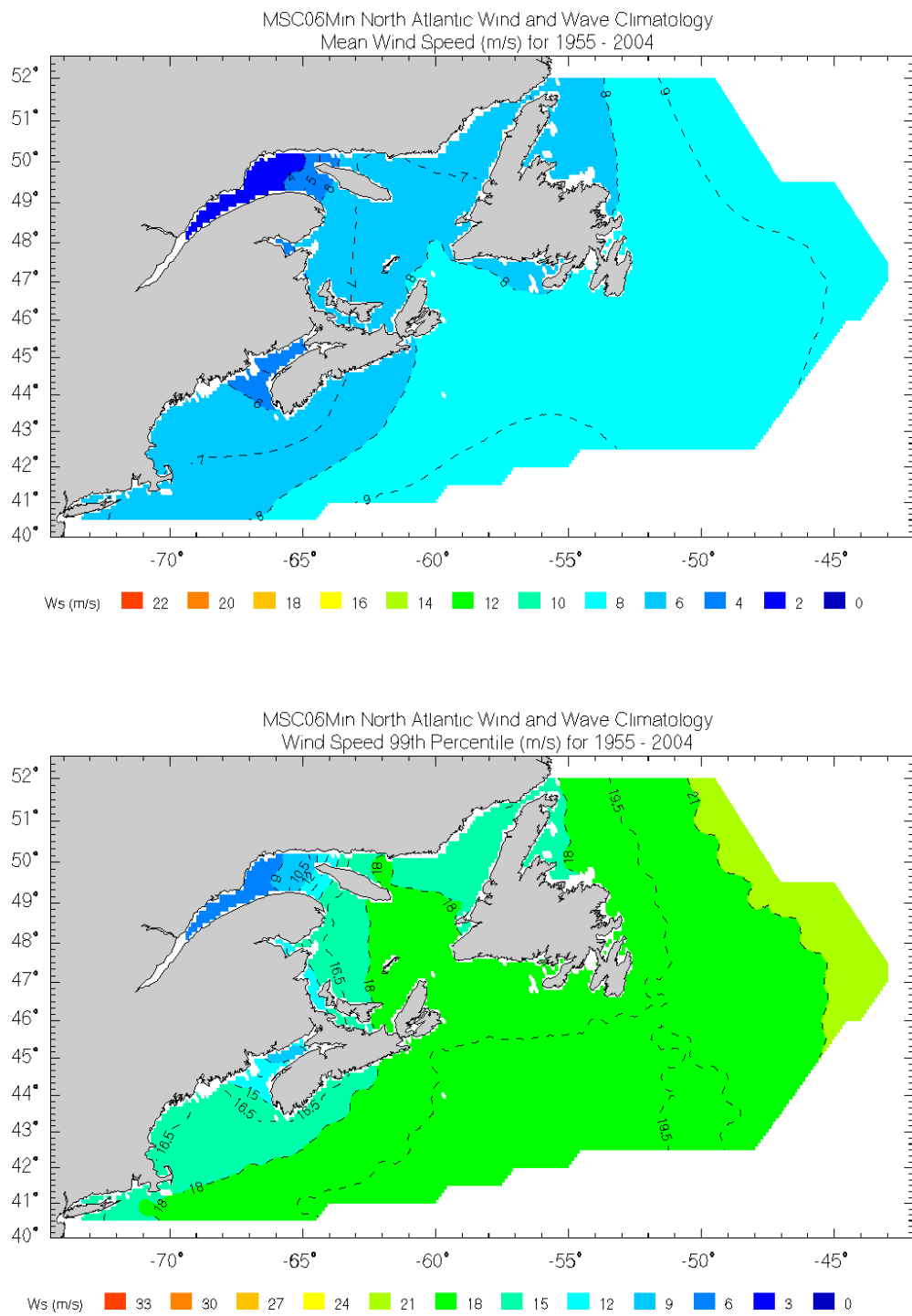


Figure 17. Wind speed statistics over the period 1955-2004: annual mean wind speed (top); 99<sup>th</sup> percentile wind speed (bottom)

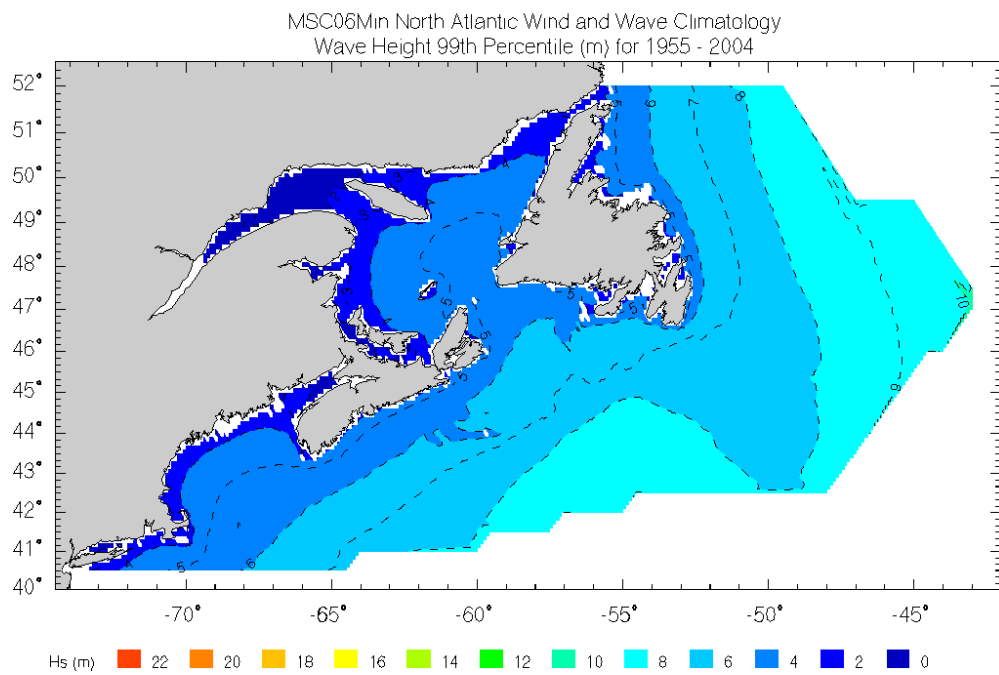
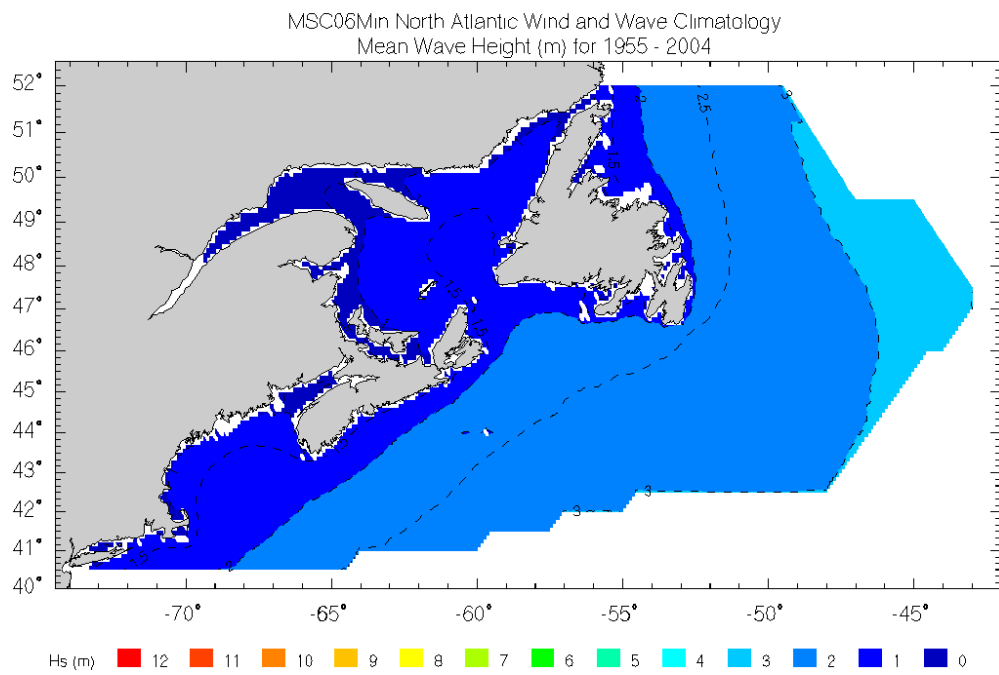


Figure 18. Wave height statistics over the period 1955-2004: annual mean wave height (top); 99<sup>th</sup> percentile wave height (bottom)

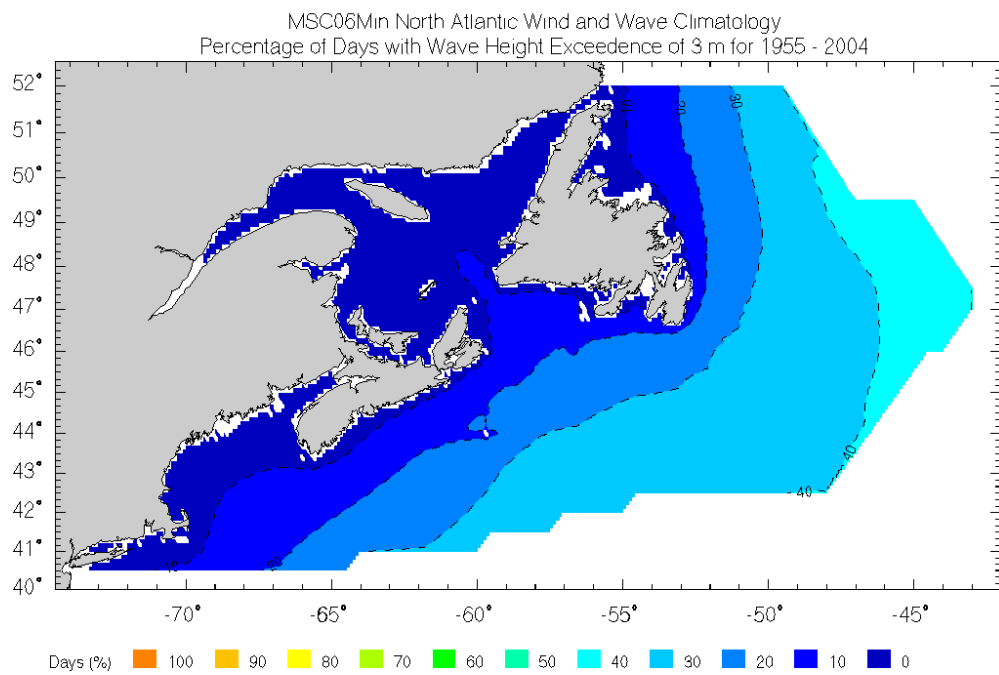
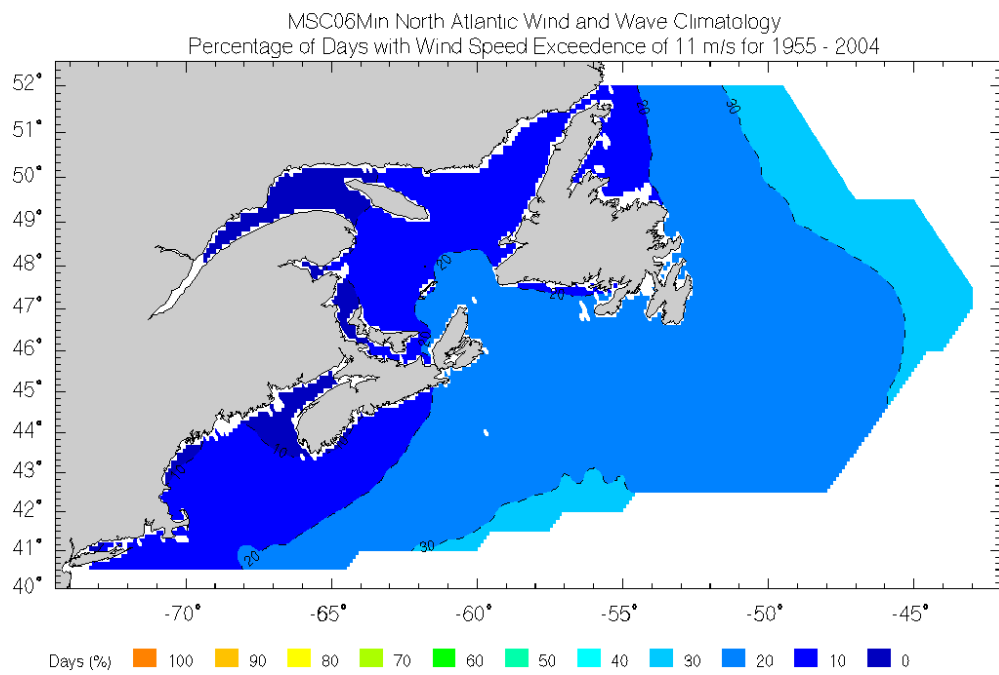


Figure 19. Percentage of days wind speed exceeded 11 m/s (top) and wave heights exceeded 3 meters (bottom)

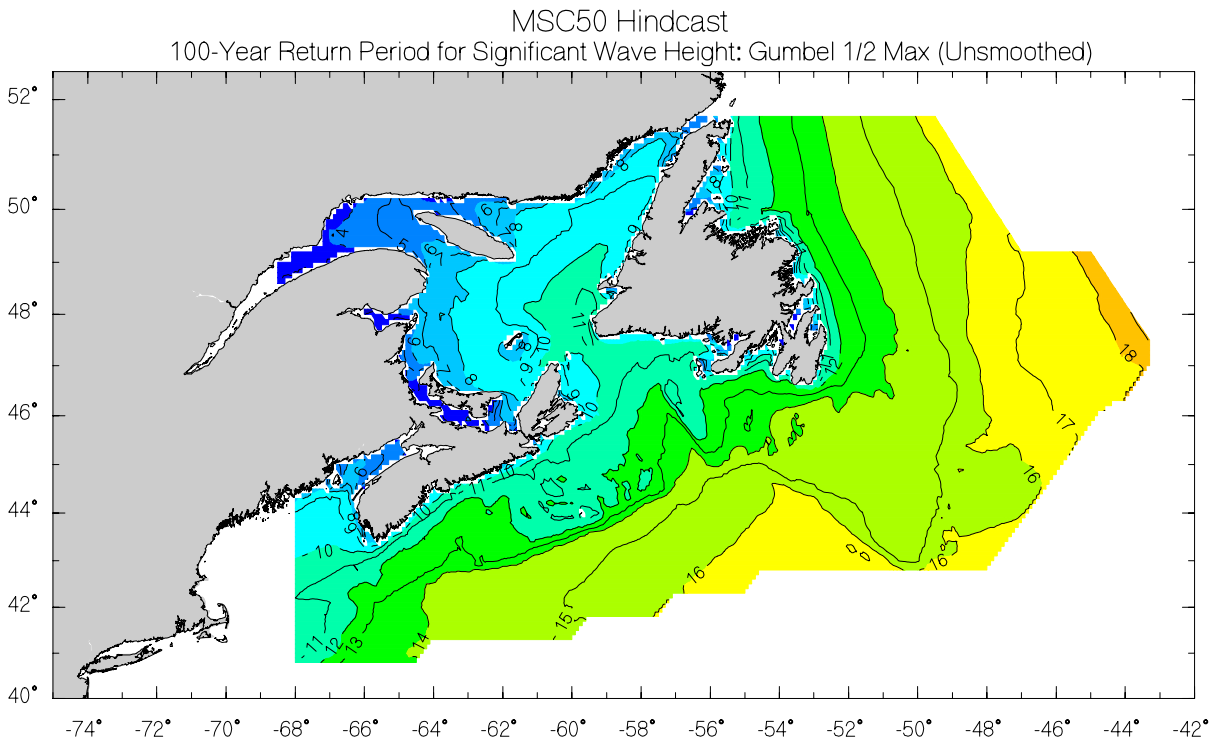
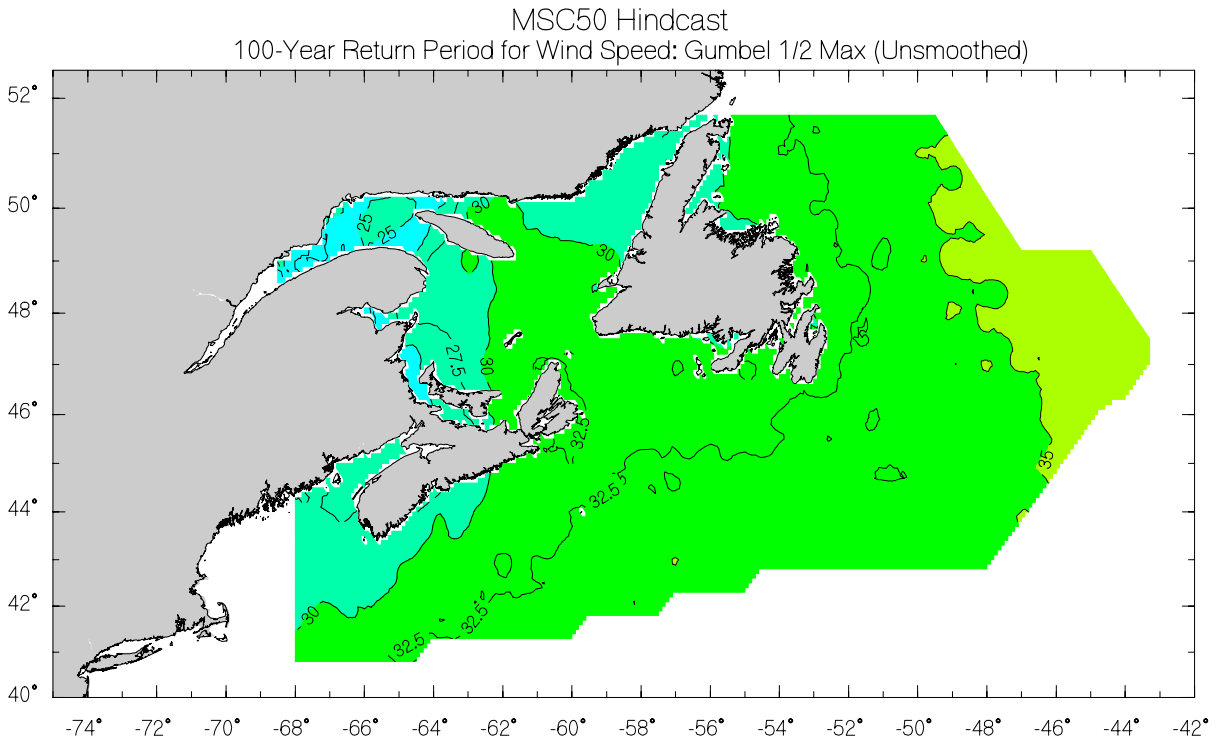


Figure 20. 100-year return period winds (m/s, top) and waves (m, bottom) computed from MSC06Min hindcast applying a 1/2 max threshold and Gumbel distribution.

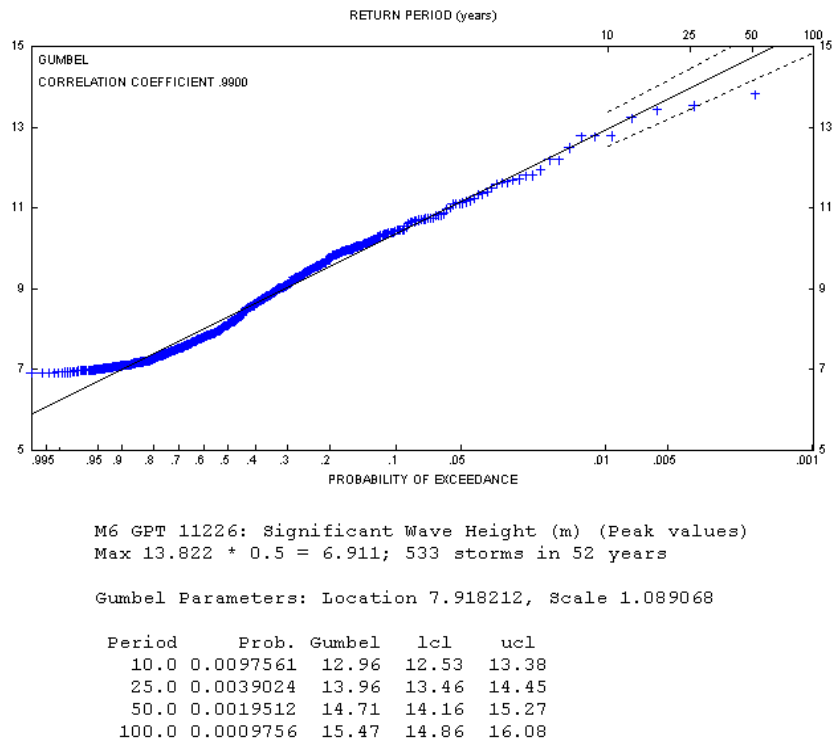
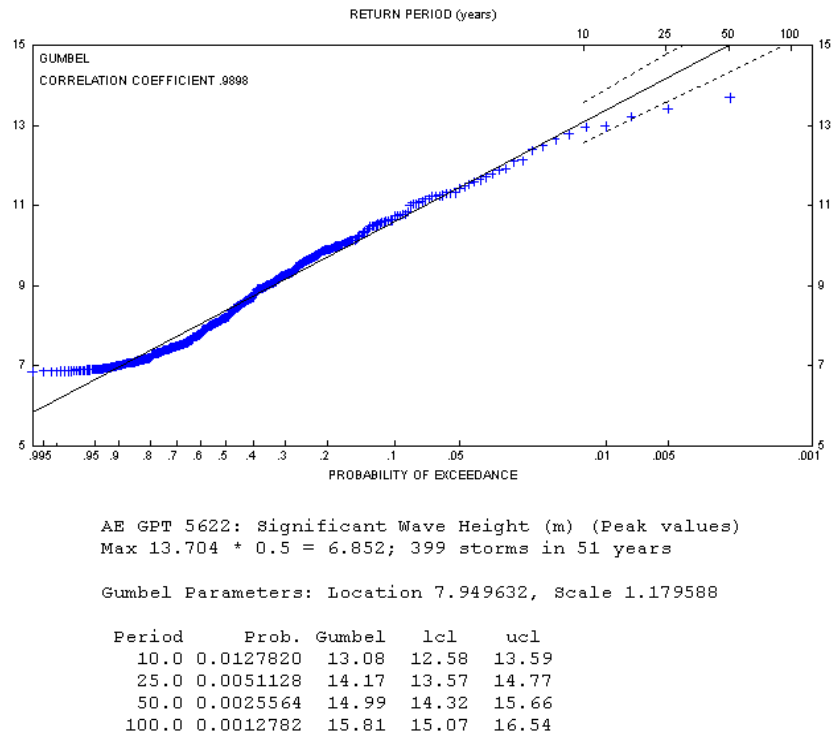


Figure 21. Gumbel distribution fits to the AES40 significant wave height (m, top) and MSC50 significant wave height (m, below) at the nearest location to the Hibernia platform.

## 5. SUMMARY

This study describes the second generation engineering-quality 50-year wind and wave hindcast produced for the entire North Atlantic Ocean using a long term, consistent wind field forcing based on improvements on the AES40 hindcast.

*In situ* and satellite observations have been used to evaluate the wind and wave hindcast. The hindcast compares well against the available buoy, platform, ocean weather ship and satellite measurements in all parts of the North Atlantic, not only in terms of bias and scatter, but over the entire frequency distribution out to and beyond the 99<sup>th</sup> percentiles of both winds and waves. Comparisons of *in situ* data over the full 1954-2005 period show that the hindcast has remained consistent with the observations. The wind and wave data are considered to be of sufficiently high quality to be used in the analysis of long return period statistics, and other engineering applications.

When the MSC50 basin hindcast is compared to the original AES40 hindcast using *insitu* observations the results show similar wave height bias (0.10 to 0.08 m) and with scatter index reduction by 43% (0.23 to 0.16). Comparison of the two hindcasts using altimeter data also show similar bias (-0.01 to 0.04) with reduction in scatter index of 29% (0.22 to 0.17).

## ACKNOWLEDGEMENTS

The authors would like to thank Canadian Hydrological Service and Canadian Ice Service who both provided valuable data applied in the MSC50 hindcast. All work for the MSC50 project was funded by the Climate Research Division of Environment Canada and the Federal Program of Energy Research and Development.

## 6. REFERENCES

- Cardone, V. J., D. Szabo and F. J. Dello Stritto. 1989. *Development of extreme wind and wave criteria for Hibernia*. Second International Workshop on Wave Hindcasting and Forecasting, April 25-28, 1989, Vancouver, Canada.
- Cardone, V.J., H.C. Graber, R.E. Jensen, S. Hasselmann, and M.J. Caruso, 1995. *In search of the true surface wind field in SWADE IOP-1: ocean wave modeling perspective*. The Global Ocean Atmosphere System, **3**, 107-150.
- Cardone, V.J., J.G. Greenwood and M.A. Cane, 1990. *On trends in historical marine wind data*. J. Climate, **3**, 113-127.
- Cardone, V.J., R.E. Jensen, D.T. Resio, V.R. Swail and A.T. Cox, 1996. *Evaluation of Contemporary Ocean Wave Models in Rare Extreme Events: "Halloween Storm of October, 1991; "Storm of the Century" of March, 1993."* J. Atmos. Ocean. Tech., **13**, 1, 198-230.
- Caires, A., A. Sterl, A. Bidlot, N. Graham and V.R. Swail 2004. *Intercomparison of Different Wind-Wave Reanalyses*. Journal of Climate Vol.17, Issue 10, pp. 1893-1913.
- Cotton, P.D., and D.J.T. Carter, 1994. *Cross calibration of TOPEX, ERS-1, and Geosat wave heights*. J. of Geophysical Research, **99**, C12, 25,025-25,033.
- Cox, A.T., and V.R. Swail, 2001. *A global wave hindcast over the period 1958-1997: validation and climate assessment*. J. of Geophys. Res.
- Cox, A.T., J.A. Greenwood, V.J. Cardone and V.R. Swail, 1995. *An interactive objective kinematic analysis system*. Proceedings 4th International Workshop on Wave Hindcasting and Forecasting, October 16-20, 1995, Banff, Alberta, p. 109-118.
- Donelan, M. A., B. K. Haus, N. Reul, W.J. Plant, M. Stiassnie, H. C. Graber, O.B. Brown and E.S. Saltzman, 2004. *On the limiting aerodynamic roughness of the ocean in very strong winds*. Geophys. Res. Letts., Vol. 31, L18306, 1-5.
- Forristall, G.Z. and J. A. Greenwood, 1998. *Directional spreading of measured and hindcasted wave spectra*. Proc. 5<sup>th</sup> International Workshop on Wave Hindcasting and Forecasting, Melbourne, FL, January 26-30, 1998.
- Greenwood, J.A., V.J. Cardone and L.M. Lawson, 1985. *Intercomparison test version of the SAIL wave model*. Ocean Wave Modelling, the SWAMP Group, Plenum Press, 221-233.
- Gumbel, E.J. 1958. *Statistics of Extremes*. Columbia University Press, New York, 375 pp.
- Khandekar, M.L., R. Lalbeharry and V.J. Cardone, 1994. *The Performance of the Canadian Spectral Ocean Wave Model (CSOWM) During the Grand Banks ERS-1 SAR Wave Spectra Validation Experiment*. Atmosphere-Ocean, **32**, 1, 31-60.
- Komen, G. J., S. Hasselmann and K. Hasselmann, 1985. "On the existence of a fully developed windsea spectrum". *J.Phys.Oceanog.*, **14**, 1271-1285.
- Hasselmann, S. and K. Hasselmann, 1985. *Computations and parameterizations of the nonlinear energy transfer in gravity wave*

- spectrum. Part I: A new method for efficient computations of the exact nonlinear transfer integral. *J. Phys. Oceanogr.*, **12**, 1369-1377.
- Powell, M. D, P. J. Vickery and T. A. Rheinhold, 2003. Reduced drag coefficient for high wind speeds in tropical cyclones. *Nature*. Vol. 422, March 20, 279-283.
- Snyder, R., F.W. Dobson, J.A. Elliott and R.B. Long, 1981. *Array measurements of atmospheric pressure fluctuations above surface gravity waves*. *J. Fluid Mech.*, **102**, 1-59.
- Swail, V.R., V.J. Cardone and B. Eid, 1989. *An Extremes Wind and Wave Hindcast off the East Coast of Canada*. Proc. 2<sup>nd</sup> Int'l Workshop on Wave Hindcasting and Forecasting. Vancouver, BC: 151-160.
- Swail, V.R. and A.T. Cox, 2000. *On the use of NCEP/NCAR reanalysis surface marine wind fields for a long term North Atlantic wave hindcast*. *J. Atmos. Ocean. Technol.*, **17**, 532-545.
- Swail, V.R., M. Parsons, B.T. Callahan and V.J. Cardone, 1995. *A revised extreme wave climatology for the east coast of Canada*. Proceedings 4th International Workshop on Wave Hindcasting and Forecasting, October 16-20, 1995, Banff, Alberta, p. 81-91.
- Swail, V.R., E.A. Ceccacci and A.T. Cox, 2000. *The AES40 North Atlantic Wave Reanalysis: Validation and Climate Assessment*. 6<sup>th</sup> International Workshop on Wave Hindcasting and Forecasting. Nov. 6-10, 2000, Monterey, CA.
- Walsh, J.E., and C.M. Johnson, 1979. *An analysis of Arctic sea ice fluctuations, 1953-1977*. *J. Phys. Ocean.*, **9**, 580-591.
- WAMDI Group, 1988. *The WAM model - a third generation ocean wave prediction model*. *J. Phys. Ocean.* **18**: 1775-1810.
- Woolf, D.K., P.G. Challenor and P.D. Cotton, 2002. Variability and predictability of North Atlantic wave climate. *J. Geo. Res.* Vol 107, No.0.
- Worley, S.J., S.D. Woodruff, R.W. Reynolds, S.J. Lubker, and N. Lott, 2005: *ICOADS Release 2.1 data and products*. *Int. J. Climatol.* (CLIMAR-II Special Issue), **25**, 823-842 (DOI: 10.1002/joc.1166).
- Wu, J., 1982. *Wind-stress coefficients over the sea surface from breeze to hurricane*. *J. Geophys. Res.*, **87**, 9704-9706.